An HDG method for non-matching meshes

Ngoc-Cuong Nguyen * Jaime Peraire † Manuel Solano ‡ Sébastien Terrana §

April 17, 2020

Abstract

We present a hybridizable discontinuous Galerkin (HDG) method for non-matching meshes. The method is devised by formulating HDG discretizations on the non-matching meshes and gluing these HDG discretizations through appropriate transmission conditions that weakly enforce the continuity of the numerical trace and the numerical flux across the non-matching meshes. The transmission conditions are based upon transferring the numerical flux from the first mesh to the second mesh and the numerical trace from the second mesh to the first mesh. The transfer of the numerical trace/flux from one mesh to the other mesh relies on the extrapolation of the approximate flux and is made to be consistent with the HDG methodology for conforming meshes. Stability of the HDG method is shown and the error analysis of the HDG method is established. Numerical results are presented to validate the theoretical results.

1 Introduction

In different applications, interfaces divide the domain of interest $\Omega \subset \mathbb{R}^d$ ($d = 2, 3$) into several subdomains. For instance, elliptic interface problems [11] where the partial differential equation (PDE) is characterized by jumps of its solution across the interfaces, or situations where different PDEs are coupled at the interfaces through different transmission conditions. In these situations, the discretization of a subdomain may not *match* the discretization of its neighboring subdomains. For example, in the case of solid-fluid interactions, it is desirable to have a finer mesh in the region occupied by the fluid, compared to the meshsize of the discretization of the solid. In addition to the mismatch due to the non-conformity, if the interfaces separating the domain Ω are not polyhedral, there would be *gap* (part of the domain which is not meshed) between the triangulations of each subdomain, as we see in the example display in Figure 1. Another application arises from the domain decomposition method where the mesh in the different subdomains of the domain do not necessarily match at their common interface.

A wide variety of methods for piecewise flat interfaces problems can be found in the literature, in contrast to those dealing with non-matching meshes. Certainly, numerical methods based on finite element approximations that deal with curved interfaces and non-matching grids are not new. In fact, one of the first approaches in the literature were based on curvilinear maps such as isoparametric finite elements [1, 12]. The mesh in these type of methods is composed by polyhedral partition where some of the elements have a curved side that interpolates the interface. In general, methods involving curvilinear mappings are computationally expensive because they require to compute non-linear mappings to construct the basis functions of the discrete spaces associated to the elements near the interface. Moreover, their precision depends on the accuracy of the interpolation spline. In the same direction, isogeometric analysis using NURBS as basis functions can be also used for interface conditions imposing higher–order continuity across the interface [9].

An alternative to curvilinear methods is to consider polytopal meshes that not necessarily are adjusted to the interface. However, the effect of the variational crime of this approach is more significant than that

*Department of Aeronautics and Astronautics, Massachusetts Institute of Technology, Cambridge, Massachusetts, USA.

†Department of Aeronautics and Astronautics, Massachusetts Institute of Technology, Cambridge, Massachusetts, USA.

‡Departamento de Ingeniería Matemática and Centro de Investigación en Ingeniería Matemática (CI^2MA), Universidad de Concepción, Concepción, Chile.

§Department of Aeronautics and Astronautics, Massachusetts Institute of Technology, Cambridge, Massachusetts, USA.

of isoparametric elements. Several methods overcome this lack of accuracy due to the poor approximation of the interface. For example, Mortar methods [10] where a Lagrange multiplier is considered to weakly impose the transmission condition across the curved interface. However, their main drawback is the low order approximation of the solution. Recently, a novel approach provides a high order method for problems involving curved interfaces approximated by polytopal meshes [2]. It is based on the Polynomial Extension Finite Element Method (PE-FEM) originally developed in the context of boundary value problems [3]. Roughly speaking, instead of adjusting the mesh to the interface, PE-FEM forces a polynomial extension of the approximate solution to match the prescribed Neumann or Dirichlet boundary condition. Actually, polynomial extensions have been also used during the last decade, mostly in the context of hybridizable discontinuous Galerkin (HDG) methods [6, 7, 8, 13]. There, the polynomial approximation of the gradient of the solution is extended outside the computational domain, whereas the solution is extended by integrating the polynomial approximation of the gradient along *transferring segments* connecting the computational boundary/interface and the boundary/interface of the domain. We consider the latter approach because of its flexibility to deal also with situations where the mesh do not interpolate the interface as in the case of immerse-type methods. For example, in Figure 2 both meshes are *far* from the interface.

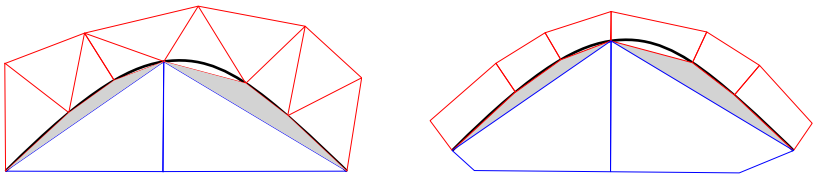

Figure 1: Example of non-matching meshes in two-dimension made of triangles (left) and quadrilaterals (right). The red mesh in finer than the blue one and the shaded regions (gap) are not meshed. The black-solid line is the interface.

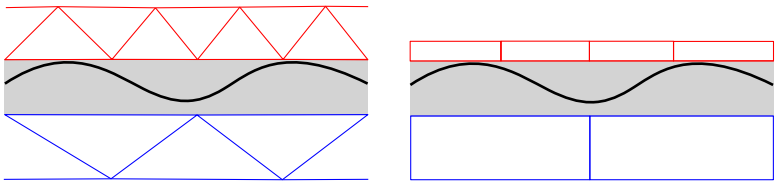

Figure 2: Same as Figure 1, but considering unfitted meshes.

Based on the transferring technique of [6], this work proposes and analyses a new method to handle situations where the discretizations of different regions of the domain do not match as in the examples depicted in Figures 1 and 2. For the sake of simplicity of the analysis and the exposition, we consider the following diffusion problem:

$$\boldsymbol{q} + \nabla u = 0 \quad \text{in} \quad \Omega, \tag{1a}$$

$$-\nabla \cdot \boldsymbol{q} = f \quad \text{in} \quad \Omega, \tag{1b}$$

$$u = 0 \quad \text{on} \quad \Gamma := \partial\Omega, \tag{1c}$$

where $\Omega \subset \mathbb{R}^d$ $(d = 2, 3)$ is a polyhedral domain, $f \in L^2(\Omega)$ is a given source term, u and $\boldsymbol{q}$ are the unknowns. Since we are interested in the regions where the meshes do not match, here we have only considered homogeneous Dirichlet boundary conditions, but other type of boundary conditions can be also considered without difficulties. Even though this is a simple model, it poses several technicalities for theoretical analysis that need to be understood before considering more complex problems.

The remainder of the manuscript is organized as follows. In Section 2, we introduce the HDG method for solving the problem 1 on non-matching meshes. Next, we show the stability of the method in Section 3 and present *a prior* error analysis in Section 4. Finally, Numerical results are presented in Section 5 to validate the theoretical results.

2 The method

2.1 Notation

The Computational Domain. The physical domain Ω consists of two disjoint open subdomains Ω^1 and Ω^2 such that $\mathcal{I} := \overline{\Omega^1} \cap \overline{\Omega^2}$ represents the interface between the two subdomains. For $i \in \{1, 2\}$ and $h_i > 0$, let $\Omega^i_{h_i} = \{K\}$ denote a $(\Gamma \cap \partial\Omega^i)$-conforming triangulation of Ω^i, with boundary $\Gamma^i_{h_i}$, made of polyhedral elements K of size proportional to h_i. Without loss of generality we suppose $h_2 > h_1$. We assume each element K is a simplex, a quadrilateral ($d = 2$) or a hexahedron ($d = 3$). Also, to simplify notation, we will just write h instead of h_i when there is no confusion, i.e., when the label h indicates the size of the triangulation Ω^1_h or Ω^2_h. In this case, $\overline{\Omega^1_h} \cap \overline{\Omega^2_h}$ is not necessarily $\mathcal{I}$ as in the examples displayed in Figures 1 and 2. Then, for $i = 1, 2$ we define $\mathcal{I}^i_h := \Gamma^i_h \setminus \Gamma$ (see Figure 3 for an illustration).

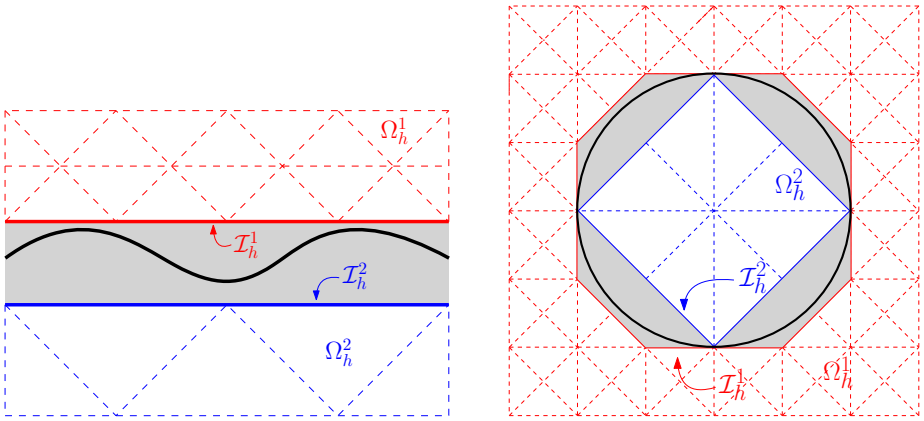

Figure 3: Examples of computational domain and notation.

The family of triangulations $\{\Omega^i_h\}_{h>0}$ is assumed to be shape-regular, i.e., there exists $\beta_i > 0$ such that for all elements $K \in \Omega^i_h$ and all $h > 0$, $h_K/\rho_K \leq \beta_i$, where h_K is the diameter of K and ρ_K is the diameter of the largest ball contained in K. For every element K, we will denote by $\boldsymbol{n}_K$ the outward unit normal vector to K, writing $\boldsymbol{n}$ instead of $\boldsymbol{n}_K$ when there is no confusion. The set of all the faces of Ω^i_h is denoted by $\mathcal{E}^i_h$.

Spaces and norms. Given an element K and a non-negative integer r, $\mathbb{P}_r(K)$ denotes the space of polynomials of total degree at most r, and we define $\mathbf{P}_r(K) := [\mathbb{P}_r(K)]^d$. Given a region $D \subset \mathbb{R}^d$, we denote by $(\cdot,\cdot)_D$ and $\langle\cdot,\cdot\rangle_{\partial D}$ the $L^2(D)$ and $L^2(\partial D)$ inner products, respectively. The L^2-norms over D and ∂D will be denoted by $\|\cdot\|_D$ and $\|\cdot\|_{\partial D}$. We use the standard notation for Sobolev spaces and their associated norms and seminorms, where vector-valued functions and their corresponding spaces are denoted in bold face.

The inner products for the triangulation Ω^i_h $(i = 1, 2)$ are given by

$$(\cdot,\cdot)_{\Omega^i_h} := \sum_{K\in\Omega^i_h} (\cdot,\cdot)_K, \qquad \langle\cdot,\cdot\rangle_{\partial\Omega^i_h} := \sum_{K\in\Omega^i_h} \langle\cdot,\cdot\rangle_{\partial K} \quad \text{and} \quad \langle\cdot,\cdot\rangle_{\mathcal{I}^i_h} := \sum_{e\in\mathcal{I}^i_h} \langle\cdot,\cdot\rangle_e,$$

and their corresponding norms will be denoted, respectively, by

$$\|\cdot\|_{\Omega^i_h} := \left(\sum_{K\in\Omega^i_h} \|\cdot\|^2_K\right)^{1/2}, \qquad \|\cdot\|_{\partial\Omega^i_h} := \left(\sum_{K\in\Omega^i_h} \|\cdot\|^2_{\partial K}\right)^{1/2} \quad \text{and} \quad \|\cdot\|_{\mathcal{I}^i_h} := \left(\sum_{e\in\mathcal{I}^i_h} \|\cdot\|^2_e\right)^{1/2}.$$

To avoid proliferation of unimportant constants, we will use the terminology $a \lesssim b$ whenever $a \leq Cb$ and C is a positive constant independent of h.

Connecting segments. For each point $\boldsymbol{x}^2 \in \mathcal{I}_h^2$, we associate a point $\boldsymbol{x}^1 \in \mathcal{I}_h^1$. We denote by $\sigma(\boldsymbol{x}^2)$ the segment starting at $\boldsymbol{x}^2$ and ending at $\boldsymbol{x}^1$, with unit tangent vector $\boldsymbol{m}$ and length $|\sigma(\boldsymbol{x}^2)|$. The segment $\sigma(\boldsymbol{x}^2)$ is referred as the *connecting segment* associated to $\boldsymbol{x}^2$ and is assumed to satisfy two conditions: it does not intersect the interior of another segment and its length $|\sigma(\boldsymbol{x}^2)|$ is of order at most $\max\{h_1, h_2\} = h_2$, where we recall that h_i is the mesh size of the triangulation Ω_h^i that satisfies $h_2 > h_1$.

Now, let $\boldsymbol{v}^2$ a vertex of $\mathcal{I}_h^2$. We assume that the point $\boldsymbol{v}^1$ associated to $\boldsymbol{v}^2$ is a vertex of $\mathcal{I}_h^1$. In Figures 1-3 this is always the case. Then, $\mathcal{I}_h^1$ induces a partition of $\mathcal{I}_h^2$ that we denoted by $\mathcal{F}_h^2 = \{e\}$.

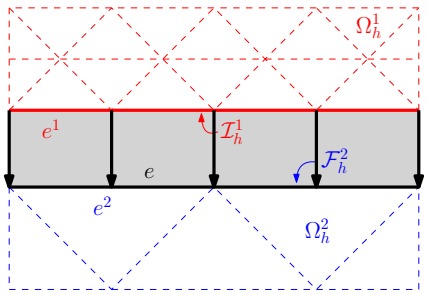

Figure 4: $\mathcal{F}_h^2$ is the partition of $\mathcal{I}_h^2$ induced by $\mathcal{I}_h^1$. In this illustration, $e^2 \in \mathcal{I}_h^2$ is partitioned in two faces.

Extrapolation operator. The region enclosed by Ω_h^1 and Ω_h^2 (shaded area in Figures 1-3) will be denoted by Ω_h^{ext}. We notice that Ω_h^{ext} is not meshed. As a consequence, we don't have an HDG approximation in there. That is why the HDG approximation of the flux $\boldsymbol{q}$ will be locally extrapolated from the computational domain $\Omega_h^1 \cup \Omega_h^2$ to Ω_h^{ext}. More precisely, let $\boldsymbol{p}|_K : \mathbf{P}_k(K) \to \mathbb{R}$ be a vector-valued polynomial function which is defined on an element K in $\Omega_h^1 \cup \Omega_h^2$ such that $\overline{K} \cap \overline{\Omega_h^{ext}} \neq \emptyset$. We will define its extension to Ω_h^{ext} as

$$\boldsymbol{E}_{\boldsymbol{p}|_K}(\boldsymbol{y}) := \boldsymbol{p}|_K(\boldsymbol{y}) \qquad \forall\, \boldsymbol{y} \in \Omega_h^{ext}. \tag{2}$$

Note that the extended function $\boldsymbol{E}_{\boldsymbol{p}|_K}(\boldsymbol{y})$ is a vector-value polynomial function whose support includes Ω_h^{ext}. Each element K will have its own extended function.

The HDG-projection. In the analysis we will employ the HDG projection devised in [4]. More precisely, let τ be the stabilization parameter of the HDG method that we assume non-negative and uniformly bounded. For $i \in \{1, 2\}$ and a pair of functions $(\boldsymbol{q}^i, u^i) \in \boldsymbol{H}^1(\Omega_h^i) \times H^1(\Omega_h^i)$, we recall its HDG projection $\boldsymbol{\Pi}^i(\boldsymbol{q}^i, u^i) := (\boldsymbol{\Pi}_{\boldsymbol{V}^i}\boldsymbol{q}^i, \Pi_{W_i}u^i) \in \boldsymbol{V}_h^i \times W_h^i$ defined as the unique element-wise solution of

$$(\boldsymbol{\Pi}_{\boldsymbol{V}^i}\boldsymbol{q}^i, \boldsymbol{v})_K = (\boldsymbol{q}^i, \boldsymbol{v})_K \qquad \forall\, \boldsymbol{v} \in \mathbf{P}(K), \tag{3a}$$

$$(\Pi_{W^i}u, w)_K = (u, w)_K \qquad \forall\, w \in \mathbb{P}_{k-1}(K), \tag{3b}$$

$$\langle \boldsymbol{\Pi}_{\boldsymbol{V}^i}\boldsymbol{q} \cdot \boldsymbol{n}^i + \tau\Pi_{W^i}u^i, \mu\rangle_F = \langle \boldsymbol{q}^i \cdot \boldsymbol{n}^i + \tau u^i, \mu\rangle_F \qquad \forall\, \mu \in \mathbb{P}_k(F), \tag{3c}$$

for every element $K \in \Omega_h^i$, and $F \in \partial\Omega_h^i$. Here $\boldsymbol{V}_h^i$ and W_h^i are the HDG spaces consisting of polynomials of degree at most k on each element K. In addition, the L^2 projection into M_h^i will be denoted as P_{M^i} and, given constants $l_{\boldsymbol{q}}$ and $l_u \in [0, k]$, if $(\boldsymbol{q}^i, u^i) \in \boldsymbol{H}^1(\Omega_h^i) \times H^1(\Omega_h^i) \in H^{l_{\boldsymbol{q}}+1}(\Omega_h^i) \times H^{l_u+1}(\Omega_h^i)$ and the stabilization function is chosen so that $\tau_K^{\max} := \max \tau|_{\partial K} > 0$, then by [4] and [5],

$$\|\boldsymbol{\Pi}_{\boldsymbol{V}^i}\boldsymbol{q}^i - \boldsymbol{q}^i\|_K \lesssim h_K^{l_{\boldsymbol{q}}+1}|\boldsymbol{q}^i|_{\boldsymbol{H}^{l_{\boldsymbol{q}}+1}(K)} + h_K^{l_u+1}|u^i|_{H^{l_u+1}(K)}, \tag{4a}$$

$$\|\Pi_{W^i}u^i - u^i\|_K \lesssim h_K^{l_u+1}|u^i|_{H^{l_u+1}(K)} + h_K^{l_{\boldsymbol{q}}+1}|\nabla \cdot \boldsymbol{q}^i|_{H^{l_{\boldsymbol{q}}}(K)}, \tag{4b}$$

for all $K \in \Omega_h^i$.

Further notation and auxiliary estimates. Given a face $e \in \mathcal{I}_h^2$ belonging to the element $K_e \in \Omega_h^2$, we define the *extrapolation patch* as

$$K_e^{ext} := \{\boldsymbol{x} + \boldsymbol{n}^2 t : 0 \le t \le |\sigma(\boldsymbol{x})|, \boldsymbol{x} \in e\}. \tag{5}$$

We denote by $h_e^\perp$ (resp. $H_e^\perp$) the largest distance of a point inside K_e (resp. K_e^{ext}) to the the plane determined by the face e. In other words,

$$h_e^\perp = \max_{\boldsymbol{x}\in K_e} |\mathrm{dist}(\boldsymbol{x}, e)|, \qquad H_e^\perp = \max_{\boldsymbol{x}\in e} |\sigma(\boldsymbol{x})|, \tag{6}$$

where $\mathrm{dist}(\boldsymbol{x}, e)$ denotes the distance from $\boldsymbol{x}$ to the face e. We set the ratio $r_e := H_e^\perp / h_e^\perp$ and its maximum

$$R_2 := \max_{e\in\mathcal{I}_h^2} r_e. \tag{7}$$

We also define

$$\boldsymbol{\mathcal{V}}^k := \left\{ \boldsymbol{p} \in [\mathbb{P}_k(K_e^{ext})]^d \,,\, \boldsymbol{p} \neq \boldsymbol{0} \right\},$$

and we denote by $\boldsymbol{n}_e$ the interior normal vector to K_e^{ext} along the edge e, i.e. the exterior normal vector to K_e pointing in the direction of K_e^{ext}. We can then introduce the constants

$$C_e^{ext} := \frac{1}{\sqrt{r_e}} \sup_{\boldsymbol{\chi}\in\boldsymbol{\mathcal{V}}^k} \frac{\|\boldsymbol{\chi}\cdot\boldsymbol{n}_e\|_{K_e^{ext}}}{\|\boldsymbol{\chi}\cdot\boldsymbol{n}_e\|_{K_e}}, \qquad C_e^{inv} := h_e^\perp \sup_{\boldsymbol{\chi}\in\boldsymbol{\mathcal{V}}^k} \frac{\|\partial_{\boldsymbol{n}_e}\boldsymbol{\chi}\|_{K_e}}{\|\boldsymbol{\chi}\cdot\boldsymbol{n}_e\|_{K_e}}. \tag{8}$$

As proved in Lemma A.2 of [6], these constants are independent of the mesh size, but depend on the polynomial degree k.

On the other hand, following the ideas in [6], it is useful to introduce the following auxiliary functions. Let $e \in \mathcal{I}_h^2$ that belongs to K_e and K_e^{ext}. For a polynomial function $\boldsymbol{v}$ on K_e we define

$$\Lambda^i_{\boldsymbol{v}|_{K_e}}(\boldsymbol{x}^2) := \frac{1}{|\sigma(\boldsymbol{x}^2)|} \int_0^{|\sigma(\boldsymbol{x}^2)|} \left(\boldsymbol{E}_{\boldsymbol{v}|_{K_e}}(\boldsymbol{x}^2 + \boldsymbol{n}^2 s) - \boldsymbol{E}_{\boldsymbol{v}|_{K_e}}(\boldsymbol{x}^i) \right) \cdot \boldsymbol{n}^2 \, ds, \tag{9}$$

for $i = 1, 2$, where we recall that $\boldsymbol{x}^2 \in e$ and $\boldsymbol{x}^1 \in \mathcal{I}_h^1$ are connected by the segment $\sigma(\boldsymbol{x}^2)$. They satisfy (c.f. Lemma 5.2 in [6]):

$$\||\sigma|^{1/2}\Lambda^i_{\boldsymbol{v}|_{K_e}}\|_e \le \frac{1}{\sqrt{3}} r_e^{3/2} C_e^{ext} C_e^{inv} \|\boldsymbol{v}\|_{K_e} \qquad \forall\ \boldsymbol{v} \in \boldsymbol{V}(K_e), \tag{10a}$$

$$\||\sigma|^{1/2}\Lambda^i_{\boldsymbol{v}|_{K_e}}\|_e \le \frac{1}{\sqrt{3}} r_e \|h_e^\perp \partial_n \boldsymbol{v}\cdot\boldsymbol{n}\|_{K_e^{ext}} \qquad \forall\ \boldsymbol{v} \in \boldsymbol{H}^1(K_e^{ext}). \tag{10b}$$

These estimates will be useful for our error analysis of the HDG method. Another important tool is based on Taylor series expansion of a function defined on $\mathcal{I}_h^2$ around a point $\mathcal{I}_h^1$. More precisely, the following result holds.

Lemma 1. *Let $\boldsymbol{\phi} : \mathcal{I}_h^1 \to \mathcal{I}_h^2$ be a bijection. If $\psi \in H^2(\Omega)$ and $\boldsymbol{\varphi} := -\nabla\psi$, then*

$$\||\sigma|^{-1/2}(\psi - \psi\circ\boldsymbol{\phi}^{-1}) + |\sigma|^{1/2}(\boldsymbol{\varphi}\circ\boldsymbol{\phi}^{-1})\cdot\boldsymbol{n}^2\|_{\mathcal{I}_h^2} \lesssim R_2 h_2 \ \|\psi\|_{H^2(\Omega)}, \tag{11a}$$

$$\||\sigma|^{-1/2}(\psi - \psi\circ\boldsymbol{\phi}^{-1})\|_{\mathcal{I}_h^2} \lesssim (R_2 h_2)^{1/2} \ \|\psi\|_{H^2(\Omega)}, \tag{11b}$$

$$\||\sigma|^{-1/2}(\boldsymbol{\varphi} - \boldsymbol{\varphi}\circ\boldsymbol{\phi}^{-1})\cdot\boldsymbol{n}^2\|_{\mathcal{I}_h^2} \lesssim \|\boldsymbol{\varphi}\|_{\boldsymbol{H}^1(\Omega)}. \tag{11c}$$

Moreover, let $e \in \mathcal{I}_h^2$ with K_e the element where e belongs. If $p \in \mathbb{P}(K_e)$, then

$$\|p - p\circ\boldsymbol{\phi}^{-1}\|_e \lesssim r_e h_K^{-1/2} C_e^{ext} \|p\|_{K_e}. \tag{11d}$$

The proof is be postponed to the Appendix.

2.2 The HDG method

For a given polynomial degree k we consider the finite dimensional spaces

$$\begin{aligned}\boldsymbol{V}_h^i &:= \{\boldsymbol{v} \in \boldsymbol{L}(\Omega_h^i) : \boldsymbol{v}|_K \in \boldsymbol{V}(K),\ \forall\ K \in \Omega_h^i\},\\ W_h^i &:= \{w \in L^2(\Omega_h^i) : w|_K \in W(K),\ \forall\ K \in \Omega_h^i\},\\ M_h^i &:= \{\mu \in L^2(\mathcal{E}_h^i) : \mu|_e \in M(e),\ \forall\ e \in \mathcal{E}_h^i\},\end{aligned}$$

where the local finite dimensional spaces are $\boldsymbol{V}(K) := \mathbf{P}_k(K)$, $W(K) := \mathbb{P}_k(K)$ and $M(e) := \mathbb{P}_k(e)$.

Then, on each subdomain Ω_h^i, we seek $(\boldsymbol{q}_h^i, u_u^i, \widehat{u}_h^i) \in \boldsymbol{V}_h^i \times W_h^i \times M_h^i$ that satisfies

$$(\boldsymbol{q}_h^i, \boldsymbol{v})_{\Omega_h^i} - (u_h^i, \nabla\cdot\boldsymbol{v})_{\Omega_h^i} + \langle \widehat{u}_h^i, \boldsymbol{v}\cdot\boldsymbol{n}^i\rangle_{\partial\Omega_h^i} = 0, \tag{12a}$$

$$-(\boldsymbol{q}_h^i, \nabla w)_{\Omega_h^i} + \langle \widehat{\boldsymbol{q}}_h^i\cdot\boldsymbol{n}^i, w\rangle_{\partial\Omega_h^i} = (f, w)_{\Omega_h^i} \tag{12b}$$

$$\langle \widehat{\boldsymbol{q}}_h^i\cdot\boldsymbol{n}^i, \mu\rangle_{\partial\Omega_h^i\setminus\Gamma_h^i} = 0, \tag{12c}$$

$$\langle \widehat{u}_h^i, \mu\rangle_{\Gamma_h^i\setminus\mathcal{I}_h^i} = 0, \tag{12d}$$

for all $(\boldsymbol{v}, w, \mu) \in \boldsymbol{V}_h^i \times W_h^i \times M_h^i$, where

$$\widehat{\boldsymbol{q}}_h^i\cdot\boldsymbol{n}^i := \boldsymbol{q}_h^i\cdot\boldsymbol{n}^i + \tau(u_h^i - \widehat{u}_h^i) \qquad \text{on} \qquad \partial\Omega_h^i \tag{12e}$$

and τ is a positive stabilization function defined in $\partial\Omega_h^1\cup\partial\Omega_h^2$ assumed to be uniformly bouded. By simplicity of the exposition we assume τ is constant everywhere. The above equations must be complemented with suitable transmissions conditions across the interfaces $\mathcal{I}_h^1$ and $\mathcal{I}_h^2$ that we proceed to derive now.

In the case where the two meshes match at the interface, namely $\overline{\Omega_h^1}\cap\overline{\Omega_h^2} = \mathcal{I}$, the transmission conditions can be weakly imposed in the HDG scheme as follows [11]:

$$\langle \widehat{u}_h^1 - \widehat{u}_h^2, \mu\rangle_{\mathcal{I}} = 0, \qquad \forall\mu \in M_h(\mathcal{I}), \tag{13a}$$

$$\langle \widehat{\boldsymbol{q}}_h^2\cdot\boldsymbol{n}^2 + \widehat{\boldsymbol{q}}_h^1\cdot\boldsymbol{n}^1, \mu\rangle_{\mathcal{I}} = 0, \qquad \forall\mu \in M_h(\mathcal{I}), \tag{13b}$$

where $M_h(\mathcal{I}) := \{\mu \in L^2(\mathcal{I}) : \mu|_e \in M(e),\ \forall\,\text{face } e \text{ on } \mathcal{I}\}$. In the case where the two meshes do not match at the interface, somehow we can think that the interface $\mathcal{I}$ has been "split" in two, $\mathcal{I}_h^1$ and $\mathcal{I}_h^2$. Then, we propose to consider the following interface conditions:

$$\langle \widehat{u}_h^1 - \widetilde{u}_h^2, \mu\rangle_{\mathcal{I}_h^1} = 0, \qquad \forall\mu \in M_h(\mathcal{I}_h^1), \tag{14a}$$

$$\langle \widehat{\boldsymbol{q}}_h^2\cdot\boldsymbol{n}^2 + \widetilde{q}_h^1, \mu\rangle_{\mathcal{I}_h^2} = 0, \qquad \forall\mu \in M_h(\mathcal{I}_h^2), \tag{14b}$$

where $\widetilde{u}_h^2$ and $\widetilde{q}_h^1$ are approximations of $u|_{\mathcal{I}_h^1}$ and $\boldsymbol{q}\cdot\boldsymbol{n}^1|_{\mathcal{I}_h^2}$, resp., that will be constructed as follows.

For $\widetilde{u}_h^2$ we employ the transferring technique in [6, 7]: Let $\boldsymbol{x}^2 \in \mathcal{I}_h^2$ and its corresponding point $\boldsymbol{x}^1 \in \mathcal{I}_h^1$. Integrating (1a) along the connecting segment $\sigma(\boldsymbol{x}^2)$, we obtain

$$u(\boldsymbol{x}^1) = u(\boldsymbol{x}^2) - |\sigma(\boldsymbol{x}^2)|\int_0^1 \boldsymbol{q}(\boldsymbol{x}(s))\cdot\boldsymbol{m}(\boldsymbol{x}(s)), ds$$

where $\boldsymbol{x}(s) = \boldsymbol{x}^2 + (\boldsymbol{x}^1 - \boldsymbol{x}^2)s$, $s \in [0,1]$ is the parametrization of $\sigma(\boldsymbol{x}^2)$. Thus, motivated by this expression, we define

$$\widetilde{u}_h^2(\boldsymbol{x}^1) := \widehat{u}_h^2(\boldsymbol{x}^2) - |\sigma(\boldsymbol{x}^2)|\int_0^1 \boldsymbol{E}_{\boldsymbol{q}_h^2}(\boldsymbol{x}(s))\cdot\boldsymbol{m}(\boldsymbol{x}(s))ds. \tag{15a}$$

Here $\boldsymbol{E}_{\boldsymbol{q}_h^2}(\boldsymbol{x})$ denotes the extension of $\boldsymbol{q}_h^2(\boldsymbol{x})$ outside the computational domain Ω_h^2. On the other hand, based on the form of the HDG numerical fluxes (12e), we define

$$\widetilde{q}_h^1(\boldsymbol{x}^2) = \boldsymbol{E}_{\boldsymbol{q}_h^1}(\boldsymbol{x}^2)\cdot\boldsymbol{n}^1 + \tau(u_h^1(\boldsymbol{x}^1) - \widehat{u}_h^1(\boldsymbol{x}^1)). \tag{15b}$$

We notice that the information from $\mathcal{I}_h^2$ is being transferred to $\mathcal{I}_h^1$ through the mapping in (15a), and the information from $\mathcal{I}_h^1$ is being transferred to $\mathcal{I}_h^2$ through the mapping in (15b). Moreover, we observe that if $\mathcal{I} = \mathcal{I}_h^1 = \mathcal{I}_h^2$, then (14) reduces to (13).

In summary, the HDG scheme (12) is now completely defined with the transmission conditions (14) and the extrapolation of the numerical trace/flux (15).

3 Stability analysis

In this section we will show, under certain assumptions, an stability estimate associated to (12). In order to use this estimate to obtain both, wellposedeness and error bounds, we consider the same problem (12), but (12a) is replaced by

$$(\boldsymbol{q}_h^i, \boldsymbol{v})_{\Omega_h^i} - (u_h^i, \nabla \cdot \boldsymbol{v})_{\Omega_h^i} + \langle \widehat{u}_h^i, \boldsymbol{v} \cdot \boldsymbol{n}^i \rangle_{\partial\Omega_h^i} = (\boldsymbol{g}^i, \boldsymbol{v})_{\Omega_h^i}, \tag{16a}$$

where $\boldsymbol{g}^i \in L^2(\Omega_h^i)$ is a given function. In particular, to show wellposedeness $\boldsymbol{g}^i$ will be $\mathbf{0}$, whereas $\boldsymbol{g}^i$ will be the projection error $\boldsymbol{q}^i - \boldsymbol{\Pi}_{\boldsymbol{V}^i}\boldsymbol{q}^i$ when proving the error estiamtes.

For simplicity of exposition in the analysis, we assume that

(A.1) $\Omega_h^1 \cap \Omega_h^2 = \emptyset$,

(A.2) there is a bijection $\boldsymbol{\phi} : \mathcal{I}_h^1 \to \mathcal{I}_h^2$, such that $\boldsymbol{\phi}(\boldsymbol{x}^1) = \boldsymbol{x}^2$,

(A.3) for each $e^1 \in \mathcal{I}_h^1$, $\boldsymbol{m} = \boldsymbol{n}^2$ (as a consequence, $\boldsymbol{m} = -\boldsymbol{n}^1$).
Assumptions (A.1) and (A.2) hold true, for instance, in the illustrations of Figures 1-3. On the other hand, (A.3) is only satisfied in situations as those depicted in Figures 2 and 3 (left). However, the estimates of this work are also true if, instead of (A.3) , we assume $1 - \boldsymbol{m} \cdot \boldsymbol{n}^1$ and $1 - \boldsymbol{m} \cdot \boldsymbol{n}^2$ are positive and small enough. But, this assumption helps us to facilitate the presentation of the ideas behind the proofs.

Moreover, for the analysis we require the following smallness assumptions related to the ratio R_2. In particular, we assume

(A.4) $\max_{e \in \mathcal{I}_h^2} r_e \leq \beta h_e^\alpha$, with α and β non-negative constants independent of the meshsize.

(A.5) $\beta\tau h_2^\alpha \max_{e \in \mathcal{I}_h^2} h_e^\perp \leq 1/9$,

(A.6) $C_1 \beta^2 h_2^{2\alpha} \max_{e \in \mathcal{I}_h^2} (C_e^{ext})^2 (\beta h_2^\alpha (C_e^{inv})^2) + \beta h_2^\alpha + 3) \leq 1/4$, where C_1 is a positive constant, independent of h_2, that will appear in Lemma 3.

(A.7) $C_2 \beta h_2^\alpha \leq 1/2$, where C_2 is a positive constant, independent of h_2, that will appear in Lemma 4.

(A.8) $6\, C_{reg}^2 \left(h_2^2 \tau R_2^2 + 2h_2^2 + h_1^2 + \frac{4}{3} R_2 h_2 \right) \leq 1/8$.

We observe that Assumption (A.4) holds true, for instance, when $\mathcal{I}_h^1$ and $\mathcal{I}_h^2$ are piecewise linear interpolations of the interface $\mathcal{I}$, i.e. $\alpha = 1$, as in the example illustrated in Figure 1. It is also satisfied when there is a gap of order h, i.e. $\alpha = 0$, as in Figures 2 and 3. On the other hand (A.5)-(A.8) are satisfied for h small enough when $\alpha > 0$.

The main result of this section is the following stability estimate.

Theorem 2. *Suppose Assumptions (A) and elliptic regularity (cf. 27) hold true. If $\alpha > 1/2$ and $h < 1$, then there exists $h_0 \in (0, 1)$, such that*

$$\sum_{i=1}^{2} \|\boldsymbol{q}_h^i\|_{\Omega_h^i}^2 + \|\tau^{1/2}(u_h^i - \widehat{u}_h^i)\|_{\partial\Omega_h^i}^2 + \||\sigma|^{-1/2} \left(\widetilde{u}_h^2 \circ \boldsymbol{\phi}^{-1} - \widehat{u}_h^2\right)\|_{\mathcal{I}_h^2}^2 \lesssim (\beta + 1) \left(\|f\|_\Omega^2 + \sum_{i=1}^{2} \|\boldsymbol{g}^i\|_{\Omega_h^i}^2 \right) \tag{17a}$$

and

$$\sum_{i=1}^{2} \|u_h^i\|_{\Omega_h^i}^2 \lesssim \left(\beta \left(h_2^{2\alpha-1} + h_2^{\alpha+1} +\right) + h_1^2 + h_2^2\right) \left(\|f\|_\Omega^2 + \sum_{i=1}^{2} \|\boldsymbol{g}^i\|_{\Omega_h^i}^2 \right) + \beta h_2^{2+\alpha} \|\boldsymbol{g}^2\|_{\Omega_h^2}^2. \tag{17b}$$

Corollary 2.1. *The HDG scheme* (12) *has a unique solution.*

Proof. Let $i \in \{1,2\}$. We observe that $\boldsymbol{g}^i = 0$ in HDG scheme (12). Hence, if $f = 0$, by Theorem 2, $\boldsymbol{q}_h^i = \mathbf{0}$, $u_h^i = 0$, $\widehat{u}_h^i = 0$ and $\widetilde{u}_h^i = 0$. □

The proof of Theorem 2 is postponed to Section 3.3. To that end, we first provide two technical Lemmas.

3.1 An energy argument

We now employ an energy argument to obtain a bound for the L^2-norm of the approximation of the flux $\boldsymbol{q}_h^i$, the L^2-norm of the consistency error in the stabilization term $\tau^{1/2}(u_h^i - \widehat{u}_h^i)$ and also the L^2-norm of the term $|\sigma|^{-1/2}\left(\widetilde{u}_h^2 \circ \boldsymbol{\phi}^{-1} - \widehat{u}_h^2\right)$ which indicates the error associated to the transferred transmission condition of the scalar variable. As we will see, the right hand side of this bound depends, in addition to the sources, on terms involving the extrapolated polynomials and also on the L^2-norm of the approximation of u.

Lemma 3. *If Assumptions (A) hold, then there exists $C_1 > 0$, independent of the meshsize, such that*

$$\begin{aligned}\sum_{i=1}^{2} \|\boldsymbol{q}_h^i\|_{\Omega_h^i}^2 + &\|\tau^{1/2}(u_h^i - \widehat{u}_h^i)\|_{\partial\Omega_h^i}^2 + \||\sigma|^{-1/2}\left(\widetilde{u}_h^2 \circ \boldsymbol{\phi}^{-1} - \widehat{u}_h^2\right)\|_{\mathcal{I}_h^2}^2 \\ &\leq 12 C_1 \beta^2 h_2^{2\alpha-2} \|u_h^2\|_{\mathcal{I}_h^2}^2 + 4\|f\|_\Omega^2 + 2\sum_{i=1}^{2} \|u_h^i\|_{\Omega_h^i}^2 + 4(2+3R_2)\sum_{i=1}^{2} \|\boldsymbol{g}^i\|_{\Omega_h^i}^2. \end{aligned} \tag{18}$$

Proof. First of all, by testing equations (16a), (12b)-(12d) with

$$\boldsymbol{v} = \begin{cases} \boldsymbol{q}_h^1 & \text{in} \quad \Omega_h^1 \\ \boldsymbol{q}_h^2 & \text{in} \quad \Omega_h^2 \end{cases}, \quad w = \begin{cases} u_h^1 & \text{in} \quad \Omega_h^1 \\ u_h^2 & \text{in} \quad \Omega_h^2 \end{cases} \text{ and } \mu = \begin{cases} \widehat{u}_h^1 & \text{in} \quad \partial\Omega_h^1 \setminus \Gamma_h^1 \\ \widehat{u}_h^2 & \text{in} \quad \partial\Omega_h^2 \setminus \Gamma_h^2 \\ \widehat{\boldsymbol{q}}_h^1 \cdot \boldsymbol{n}^1 & \text{in} \quad \partial\Gamma_h^1 \setminus \mathcal{I}_h^1 \\ \widehat{\boldsymbol{q}}_h^2 \cdot \boldsymbol{n}^2 & \text{in} \quad \partial\Gamma_h^2 \setminus \mathcal{I}_h^2 \end{cases}$$

and adding them up, we obtain

$$\sum_{i=1}^{2} \|\boldsymbol{q}_h^i\|_{\Omega_h^i}^2 + \|\tau^{1/2}(u_h^i - \widehat{u}_h^i)\|_{\partial\Omega_h^i}^2 + \mathbb{T}^i = \sum_{i=1}^{2} (f, u_h^i)_{\Omega_h^i} + \sum_{i=1}^{2} (\boldsymbol{g}^i, \boldsymbol{q}_h^i)_{\Omega_h^i}, \tag{19}$$

where $\mathbb{T}^i := \langle \widehat{\boldsymbol{q}}_h^i \cdot \boldsymbol{n}^i, \widehat{u}_h^i \rangle_{\mathcal{I}_h^i}$, for $i = 1, 2$.

We now proceed to deduce how the transmission conditions (14) connect $\mathbb{T}^1$ and $\mathbb{T}^2$. More precisely, by (14a) and (15b),

$$\mathbb{T}^1 = \langle \widehat{\boldsymbol{q}}_h^1 \cdot \boldsymbol{n}^1, \widetilde{u}_h^2 \rangle_{\mathcal{I}_h^1} = \langle \boldsymbol{q}_h^1 \cdot \boldsymbol{n}^1 - (\boldsymbol{E}_{\boldsymbol{q}_h^1} \circ \boldsymbol{\phi}) \cdot \boldsymbol{n}^1 - (\widetilde{q}_h^1 \circ \boldsymbol{\phi}), \widetilde{u}_h^2 \rangle_{\mathcal{I}_h^1}.$$

We now work with the right hand side of the last expression. Let $e^1 \in \mathcal{I}_h^1$ and e its corresponding face $\mathcal{F}_h^2$. Since $\boldsymbol{\phi}$ is a bijection and $|e^1| = |e|$, we have

$$\mathbb{T}_1|_{e^1} = \langle (\boldsymbol{q}_h^1 \circ \boldsymbol{\phi}^{-1}) \cdot \boldsymbol{n}^1 - \boldsymbol{E}_{\boldsymbol{q}_h^1} \cdot \boldsymbol{n}^1 + \widetilde{q}_h^1, \widetilde{u}_h^2 \circ \boldsymbol{\phi}^{-1} \rangle_e = \mathbb{T}_{\boldsymbol{q}}^e + \langle \widetilde{q}_h^1, P_M(\widetilde{u}_h^2 \circ \boldsymbol{\phi}^{-1}) \rangle_e,$$

where $\mathbb{T}_{\boldsymbol{q}}^e := \langle (\boldsymbol{q}_h^1 \circ \boldsymbol{\phi}^{-1}) \cdot \boldsymbol{n}^1 - \boldsymbol{E}_{\boldsymbol{q}_h^1} \cdot \boldsymbol{n}^1, \widetilde{u}_h^2 \circ \boldsymbol{\phi}^{-1} \rangle_e$ and P_M is the L^2-projection on $M(e)$. Thus, by (14b),

$$\mathbb{T}_1|_{e^1} = \mathbb{T}_{\boldsymbol{q}}^e - \langle \widehat{\boldsymbol{q}}_h^2 \cdot \boldsymbol{n}^2, P_M(\widetilde{u}_h^2 \circ \boldsymbol{\phi}^{-1}) \rangle_e = \mathbb{T}_{\boldsymbol{q}}^e - \langle \widehat{\boldsymbol{q}}_h^2 \cdot \boldsymbol{n}^2, \widetilde{u}_h^2 \circ \boldsymbol{\phi}^{-1} \rangle_e$$

and then

$$\mathbb{T}_1|_{e^1} + \mathbb{T}_2|_e = \mathbb{T}_{\boldsymbol{q}}^e - \langle \widehat{\boldsymbol{q}}_h^2 \cdot \boldsymbol{n}^2, \widetilde{u}_h^2 \circ \boldsymbol{\phi}^{-1} - \widehat{u}_h^2 \rangle_e.$$

On the other hand, since by assumption ((A.2)), $\boldsymbol{m}(\boldsymbol{x}(s)) = \boldsymbol{n}^2$ for all $s \in [0,1]$, then $\boldsymbol{x}(s) = \boldsymbol{x}^2 + (\boldsymbol{x}^1 - \boldsymbol{x}^2)s = \boldsymbol{x}^2 + \boldsymbol{n}^2|\sigma(\boldsymbol{x}^2)|s$ and (15a) can be rewritten as

$$\begin{aligned}\widetilde{u}_h^2(\boldsymbol{x}^1) &= \widehat{u}_h^2(\boldsymbol{x}^2) - \int_0^{|\sigma(\boldsymbol{x}^2)|} \boldsymbol{E}_{\boldsymbol{q}_h^2}(\boldsymbol{x}^2 + \boldsymbol{n}^2 s)\cdot \boldsymbol{n}^2\, ds \\ &= \widehat{u}_h^2(\boldsymbol{x}^2) - \int_0^{|\sigma(\boldsymbol{x}^2)|} \left(\boldsymbol{E}_{\boldsymbol{q}_h^2}(\boldsymbol{x}^2 + \boldsymbol{n}^2 s)\cdot \boldsymbol{n}^2 - \boldsymbol{q}_h^2(\boldsymbol{x}^2)\cdot \boldsymbol{n}^2\right) ds - |\sigma(\boldsymbol{x}^2)|\boldsymbol{q}_h^2(\boldsymbol{x}^2)\cdot \boldsymbol{n}^2 \\ &= \widehat{u}_h^2(\boldsymbol{x}^2) - |\sigma(\boldsymbol{x}^2)|\Lambda^2_{\boldsymbol{q}_h^2}(\boldsymbol{x}^2) - |\sigma(\boldsymbol{x}^2)|\boldsymbol{q}_h^2(\boldsymbol{x}^2)\cdot \boldsymbol{n}^2,\end{aligned}$$

where we used the definition in (9). This implies that

$$\boldsymbol{q}_h^2(\boldsymbol{x}^2)\cdot \boldsymbol{n}^2 = -|\sigma(\boldsymbol{x}^2)|^{-1}(\widetilde{u}_h^2(\boldsymbol{x}^1) - \widehat{u}_h^2(\boldsymbol{x}^2)) - \Lambda^2_{\boldsymbol{q}_h^2}(\boldsymbol{x}^2). \tag{20}$$

Combining this identity with the above expression for $\mathbb{T}_1|_{e^1} + \mathbb{T}_2|_e$ and the definition of the numerical flux (12e), we obtain

$$\begin{aligned}\mathbb{T}_1|_{e^1} + \mathbb{T}_2|_e &= \mathbb{T}^e_{\boldsymbol{q}} + \langle \tau(u_h^2 - \widehat{u}_h^2), \widetilde{u}_h^2\circ\boldsymbol{\phi}^{-1} - \widehat{u}_h^2\rangle_e - \langle \boldsymbol{q}_h^2\cdot\boldsymbol{n}^2, \widetilde{u}_h^2\circ\boldsymbol{\phi}^{-1} - \widehat{u}_h^2\rangle_e \\ &= \mathbb{T}^e_{\boldsymbol{q}} + \langle \tau(u_h^2 - \widehat{u}_h^2), \widetilde{u}_h^2\circ\boldsymbol{\phi}^{-1} - \widehat{u}_h^2\rangle_e + \| |\sigma|^{-1/2}\left(\widetilde{u}_h^2\circ\boldsymbol{\phi}^{-1} - \widehat{u}_h^2\right)\|_e^2 + \langle \Lambda^2_{\boldsymbol{q}_h^2}, \widetilde{u}_h^2\circ\boldsymbol{\phi}^{-1} - \widehat{u}_h^2\rangle_e.\end{aligned}$$

Now, adding and subtracting $\widehat{u}_h$, we rewrite $\mathbb{T}^e_{\boldsymbol{q}}$ as follows:

$$\mathbb{T}^e_{\boldsymbol{q}} := \langle (\boldsymbol{q}_h^1\circ\boldsymbol{\phi}^{-1})\cdot\boldsymbol{n}^1 - \boldsymbol{E}_{\boldsymbol{q}_h^1}\cdot\boldsymbol{n}^1, \widetilde{u}_h^2\circ\boldsymbol{\phi}^{-1} - \widehat{u}_h^2\rangle_e + \langle (\boldsymbol{q}_h^1\circ\boldsymbol{\phi}^{-1})\cdot\boldsymbol{n}^1 - \boldsymbol{E}_{\boldsymbol{q}_h^1}\cdot\boldsymbol{n}^1, \widehat{u}_h^2\rangle_e,$$

which, together with (19), implies

$$\begin{aligned}\sum_{i=1}^2 \|\boldsymbol{q}_h^i\|^2_{\Omega_h^i} + \|\tau^{1/2}(u_h^i - \widehat{u}_h^i)\|^2_{\partial\Omega_h^i} + \| |\sigma|^{-1/2}\left(\widetilde{u}_h^2\circ\boldsymbol{\phi}^{-1} - \widehat{u}_h^2\right)\|^2_{\mathcal{I}_h^2} \\ = \langle (\boldsymbol{q}_h^1\circ\boldsymbol{\phi}^{-1})\cdot\boldsymbol{n}^1 - \boldsymbol{E}_{\boldsymbol{q}_h^1}\cdot\boldsymbol{n}^1, \widetilde{u}_h^2\circ\boldsymbol{\phi}^{-1} - \widehat{u}_h^2\rangle_{\mathcal{I}_h^2} - \langle \Lambda^2_{\boldsymbol{q}_h^2}, \widetilde{u}_h^2\circ\boldsymbol{\phi}^{-1} - \widehat{u}_h^2\rangle_{\mathcal{I}_h^2} \\ - \langle (\boldsymbol{q}_h^1\circ\boldsymbol{\phi}^{-1})\cdot\boldsymbol{n}^1 - \boldsymbol{E}_{\boldsymbol{q}_h^1}\cdot\boldsymbol{n}^1, \widehat{u}_h^2\rangle_{\mathcal{I}_h^2} - \langle \tau(u_h^2 - \widehat{u}_h^2), \widetilde{u}_h^2\circ\boldsymbol{\phi}^{-1} - \widehat{u}_h^2\rangle_{\mathcal{I}_h^2} \\ + \sum_{i=1}^2 (f, u_h^i)_{\Omega_h^i} + \sum_{i=1}^2 (\boldsymbol{g}^i, \boldsymbol{q}_h^i)_{\Omega_h^i}.\end{aligned}$$

Before continuing, we would like to point out that $\mathbb{T}_1 + \mathbb{T}_2$ has been decomposed in such a way that the mismatch between $\mathcal{I}_h^1$ and $\mathcal{I}_h^2$ is explicitly written in terms of $\widetilde{u}_h^2\circ\boldsymbol{\phi}^{-1} - \widehat{u}_h^2$. In the particular case when $\mathcal{I}_h^1 = \mathcal{I}_h^2$, $\widetilde{u}_h^2$ and $\widehat{u}_h^2$ coincide and therefore $\mathbb{T}_1 + \mathbb{T}_2$ vanishes.

No, by Young's inequality, with $\delta_e > 0$ at our disposal, we obtain

$$\begin{aligned}\frac{3}{4}\sum_{i=1}^2 \|\boldsymbol{q}_h^i\|^2_{\Omega_h^i} + \left(1 - \frac{3}{2}\max_{\boldsymbol{x}^2\in\mathcal{I}_h^2}(\tau^{1/2}|\sigma(\boldsymbol{x}^2)|^{1/2})\right)\|\tau^{1/2}(u_h^i - \widehat{u}_h^i)\|^2_{\partial\Omega_h^i} + \frac{1}{2}\| |\sigma|^{-1/2}\left(\widetilde{u}_h^2\circ\boldsymbol{\phi}^{-1} - \widehat{u}_h^2\right)\|^2_{\mathcal{I}_h^2} \\ \le \frac{1}{6}\||\sigma|^{1/2}((\boldsymbol{q}_h^1\circ\boldsymbol{\phi}^{-1})\cdot\boldsymbol{n}^1 - \boldsymbol{E}_{\boldsymbol{q}_h^1}\cdot\boldsymbol{n}^1)\|^2_{\mathcal{I}_h^2} + \frac{1}{2}\|\delta_e^{1/2}((\boldsymbol{q}_h^1\circ\boldsymbol{\phi}^{-1})\cdot\boldsymbol{n}^1 - \boldsymbol{E}_{\boldsymbol{q}_h^1}\cdot\boldsymbol{n}^1)\|^2_{\mathcal{I}_h^2} \\ + \frac{1}{6}\||\sigma|^{1/2}\Lambda^2_{\boldsymbol{q}_h^2}\|^2_{\mathcal{I}_h^2} + \frac{1}{2}\|\delta_e^{-1/2}\widehat{u}_h^2\|^2_{\mathcal{I}_h^2} + \|f\|^2_\Omega + \frac{1}{2}\sum_{i=1}^2\|u_h^i\|^2_{\Omega_h^i} + 2\sum_{i=1}^2\|\boldsymbol{g}^i\|^2_{\Omega_h^i}.\end{aligned} \tag{21}$$

Now, for $e \in \mathcal{I}_h^2$ by (11d), we have

$$\|(\boldsymbol{q}_h^1\circ\boldsymbol{\phi}^{-1})\cdot\boldsymbol{n}^1 - \boldsymbol{E}_{\boldsymbol{q}_h^1}\cdot\boldsymbol{n}^1\|_e \lesssim r_e h_{K_e}^{-1/2} C_e^{ext}\|\boldsymbol{q}_h^1\|_{K_e}$$

and also

$$\||\sigma|^{1/2}(\boldsymbol{q}_h^1\circ\boldsymbol{\phi}^{-1})\cdot\boldsymbol{n}^1 - \boldsymbol{E}_{\boldsymbol{q}_h^1}\cdot\boldsymbol{n}^1\|_e \lesssim r_e^{3/2} C_e^{ext}\|\boldsymbol{q}_h^1\|_{K_e},$$

where K_e is the element where e belongs. Then, from these inequalities and (10), we conclude there exists a constant $C_1 > 0$, independent of the meshsize, such that

$$\begin{aligned}\frac{3}{4}\sum_{i=1}^{2}\|\boldsymbol{q}_h^i\|_{\Omega_h^i}^2+\left(1-\frac{3}{2}\max_{\boldsymbol{x^2}\in\mathcal{I}_h^2}(\tau^{1/2}|\sigma(\boldsymbol{x}^2)|^{1/2})\right)\|\tau^{1/2}(u_h^i-\widehat{u}_h^i)\|_{\partial\Omega_h^i}^2+\frac{1}{2}\||\sigma|^{-1/2}\left(\widetilde{u}_h^2\circ\boldsymbol{\phi}^{-1}-\widehat{u}_h^2\right)\|_{\mathcal{I}_h^2}^2\\ \leq C_1\left(\max_{e\in\mathcal{I}_h^2}r_e^3(C_e^{ext}C_e^{inv})^2+\max_{e\in\mathcal{I}_h^2}r_e^3(C_e^{ext})^2+\max_{e\in\mathcal{I}_h^2}\delta_e r_e^2 h_{K_e}^{-1}(C_e^{ext})^2\right)\|\boldsymbol{q}_h^2\|_{\Omega_h^2}^2\\ +\frac{1}{2}\|\delta_e^{-1/2}\widehat{u}_h^2\|_{\mathcal{I}_h^2}^2+\|f\|\|_\Omega^2+\frac{1}{2}\sum_{i=1}^{2}\|u_h^i\|_{\Omega_h^i}^2+2\sum_{i=1}^{2}\|\boldsymbol{g}^i\|_{\Omega_h^i}^2.\end{aligned}\tag{22}$$

Thus, by choosing $\delta_e = C_1^{-1}r_e^{-2}h_{K_e}(C_e^{ext})^{-2}4^{-1}$, we have

$$\begin{aligned}\frac{1}{2}\sum_{i=1}^{2}\|\boldsymbol{q}_h^i\|_{\Omega_h^i}^2+\left(1-\frac{3}{2}\max_{\boldsymbol{x^2}\in\mathcal{I}_h^2}(\tau^{1/2}|\sigma(\boldsymbol{x}^2)|^{1/2})\right)\|\tau^{1/2}(u_h^i-\widehat{u}_h^i)\|_{\partial\Omega_h^i}^2+\frac{1}{2}\||\sigma|^{-1/2}\left(\widetilde{u}_h^2\circ\boldsymbol{\phi}^{-1}-\widehat{u}_h^2\right)\|_{\mathcal{I}_h^2}^2\\ \leq C_1\left(\max_{e\in\mathcal{I}_h^2}r_e^3(C_e^{ext}C_e^{inv})^2+\max_{e\in\mathcal{I}_h^2}r_e^3(C_e^{ext})^2\right)\|\boldsymbol{q}_h^2\|_{\Omega_h^2}^2\\ +C_1\|r_e h_{K_e}^{-1/2}C_e^{ext}\widehat{u}_h^2\|_{\mathcal{I}_h^2}^2+\|f\|\|_\Omega^2+\frac{1}{2}\sum_{i=1}^{2}\|u_h^i\|_{\Omega_h^i}^2+2\sum_{i=1}^{2}\|\boldsymbol{g}^i\|_{\Omega_h^i}^2.\end{aligned}\tag{23}$$

On the other hand, modifying the proof of Theorem 4.1 in [4], it is not difficult to show that for each $e\in\mathcal{I}_h^2$,

$$r_e h_{K_e}^{-1/2}\|\widehat{u}_h^2\|_e \lesssim r_e\|\boldsymbol{q}_h^2\|_{K_e}+r_e h_{K_e}^{-1}\|u_h^2\|_{K_e}+r_e\|\boldsymbol{g}^2\|_{K_e}.\tag{24}$$

Then, (22) implies

$$\begin{aligned}\frac{1}{2}\sum_{i=1}^{2}\|\boldsymbol{q}_h^i\|_{\Omega_h^i}^2+\left(1-\frac{3}{2}\max_{\boldsymbol{x^2}\in\mathcal{I}_h^2}(\tau^{1/2}|\sigma(\boldsymbol{x}^2)|^{1/2})\right)\|\tau^{1/2}(u_h^i-\widehat{u}_h^i)\|_{\partial\Omega_h^i}^2+\frac{1}{2}\||\sigma|^{-1/2}\left(\widetilde{u}_h^2\circ\boldsymbol{\phi}^{-1}-\widehat{u}_h^2\right)\|_{\mathcal{I}_h^2}^2\\ \leq C_1\left(\max_{e\in\mathcal{I}_h^2}r_e^3(C_e^{ext}C_e^{inv})^2+\max_{e\in\mathcal{I}_h^2}r_e^3(C_e^{ext})^2+3\max_{e\in\mathcal{I}_h^2}r_e^2(C_e^{ext})^2\right)\|\boldsymbol{q}_h^2\|_{\Omega_h^2}^2\\ +3C_1\max_{e\in\mathcal{I}_h^2}r_e^2h_{K_e}^{-2}\|u_h^2\|_{\mathcal{I}_h^2}^2+\|f\|\|_\Omega^2+\frac{1}{2}\sum_{i=1}^{2}\|u_h^i\|_{\Omega_h^i}^2+(2+3R_2)\sum_{i=1}^{2}\|\boldsymbol{g}^i\|_{\Omega_h^i}^2.\end{aligned}\tag{25}$$

The results follows by Assumptions (A.4), (A.5) and (A.6). □

We observe that we need to provide an estimate for the L^2-norm of u_h^1 and u_h^2. To that end, we will employ a duality argument.

3.2 A duality argument

Given $\Theta\in L^2(\Omega)$, we will assume that the solution $(\boldsymbol{\varphi},\psi)$ of

$$\boldsymbol{\varphi}+\nabla\psi = 0 \qquad \text{in } \Omega, \tag{26a}$$

$$\nabla\cdot\boldsymbol{\varphi} = \Theta \qquad \text{in } \Omega, \tag{26b}$$

$$\psi = 0 \qquad \text{on } \partial\Omega \tag{26c}$$

has regularity

$$\|\boldsymbol{\varphi}\|_{H^1(\Omega)}+\|\psi\|_{H^2(\Omega)}\leq C_{reg}\|\Theta\|_\Omega,\tag{27}$$

where $C_{reg}>0$ depends on the domain Ω. This result holds, for instance, for convex, polyhedral domains and for domains with C^2-boundaries.

Lemma 4. *If Assumptions (A) and* (27) *hold true, then there exists $C_2 > 0$, independent of the meshsize, such that*

$$\sum_{i=1}^{2} \|u_h^i\|_{\Omega_h^i}^2 \lesssim C_2^2 \left((R_2 h_2)^2 + R_2 h_2^2 + \beta^2 h_2^{2\alpha-1} \max_{e \in \mathcal{I}_h^2} (C_e^{ext})^2 + \frac{R_2 h_2}{2C_1} + (R_2 h_2)^2 \tau + h_1^2 + h_2^2 \right)$$
$$\left(\| |\sigma|^{-1/2} (\widetilde{u}_h^2 \circ \boldsymbol{\phi}^{-1} - \widehat{u}_h^2) \|_{\mathcal{I}_h^2}^2 + \| \tau^{1/2} (u_h^2 - \widehat{u}_h^2) \|_{\mathcal{I}_h^2}^2 + \sum_{i=1}^{2} \|\boldsymbol{q}_h^i\|_{\Omega_h^i}^2 \right) + C_2^2 R_2 h_2^2 \|\boldsymbol{g}^2\|_{\Omega_h^2}^2. \tag{28}$$

Proof. By the result of Lemma 3.3 in [6] applied to our context, it can be shown that given $\Theta \in L^2(\Omega)$ and any $\psi \in W_h$, the solution of (26) satisfies

$$\sum_{i=1}^{2} (u_h^i, \Theta)_{\Omega_h^i} = \sum_{i=1}^{2} (\boldsymbol{q}_h^i, \boldsymbol{\Pi}_{\boldsymbol{V}^i} \boldsymbol{\varphi} - \boldsymbol{\varphi})_{\Omega_h^i} + \sum_{i=1}^{2} \mathbb{T}_u^i, \tag{29}$$

where, for $i = 1, 2$, $\mathbb{T}_u^i := \langle \widehat{u}_h^i, \boldsymbol{\varphi} \cdot \boldsymbol{n}^i \rangle_{\mathcal{I}_h^i} - \langle \widehat{\boldsymbol{q}}_h^i \cdot \boldsymbol{n}^i, \psi \rangle_{\mathcal{I}_h^i}$ and $\boldsymbol{\Pi}_{\boldsymbol{V}^i}$ is the HDG projection into $\boldsymbol{V}_h^i$ defined in (3). Similarly to tjhe ideas behind the proof of Lemma 3, we will explicitly write $\mathbb{T}_u^1 + \mathbb{T}_u^2$ in terms of quantities related to the mismatch between $\mathcal{I}_h^1$ and $\mathcal{I}_h^2$. To that end, by using (14a), (15b) and mapping the integrals from $\mathcal{I}_h^1$ to $\mathcal{I}_h^2$, we have

$$\begin{aligned}
\mathbb{T}_u^1 :=& \langle \widehat{u}_h^1, \boldsymbol{\varphi} \cdot \boldsymbol{n}^1 \rangle_{\mathcal{I}_h^1} - \langle \widehat{\boldsymbol{q}}_h^1 \cdot \boldsymbol{n}^1, \psi \rangle_{\mathcal{I}_h^1} \\
=& \langle \widehat{u}_h^1, \boldsymbol{\varphi} \cdot \boldsymbol{n}^1 \rangle_{\mathcal{I}_h^1} - \langle \boldsymbol{q}_h^1 \cdot \boldsymbol{n}^1 - (\boldsymbol{E}_{\boldsymbol{q}_h^1} \circ \boldsymbol{\phi}) \cdot \boldsymbol{n}^1 + (\widetilde{q}_h^1 \circ \boldsymbol{\phi}), \psi \rangle_{\mathcal{I}_h^1} \\
=& \langle \widetilde{u}_h^2, \boldsymbol{\varphi} \cdot \boldsymbol{n}^1 \rangle_{\mathcal{I}_h^2} - \langle (\boldsymbol{q}_h^1 \circ \boldsymbol{\phi}^{-1}) \cdot \boldsymbol{n}^1 - \boldsymbol{E}_{\boldsymbol{q}_h^1} \cdot \boldsymbol{n}^1 + \widetilde{q}_h^1, \psi \circ \boldsymbol{\phi}^{-1} \rangle_{\mathcal{I}_h^2} \\
=& - \langle \widetilde{u}_h^2 \circ \boldsymbol{\phi}^{-1}, (\boldsymbol{\varphi} \circ \boldsymbol{\phi}^{-1}) \cdot \boldsymbol{n}^2 \rangle_{\mathcal{I}_h^2} + \langle (\boldsymbol{q}_h^1 \circ \boldsymbol{\phi}^{-1}) \cdot \boldsymbol{n}^2 - \boldsymbol{E}_{\boldsymbol{q}_h^1} \cdot \boldsymbol{n}^2 + \widehat{\boldsymbol{q}}_h^2 \cdot \boldsymbol{n}^2, \psi \circ \boldsymbol{\phi}^{-1} \rangle_{\mathcal{I}_h^2}.
\end{aligned}$$

Then,

$$\begin{aligned}
\mathbb{T}_u^1 + \mathbb{T}_u^2 =& \langle \widehat{u}_h^2, \boldsymbol{\varphi} \cdot \boldsymbol{n}^2 \rangle_{\mathcal{I}_h^2} - \langle \widetilde{u}_h^2 \circ \boldsymbol{\phi}^{-1}, (\boldsymbol{\varphi} \circ \boldsymbol{\phi}^{-1}) \cdot \boldsymbol{n}^2 \rangle_{\mathcal{I}_h^2} + \langle \widehat{\boldsymbol{q}}_h^2 \cdot \boldsymbol{n}^2, \psi \circ \boldsymbol{\phi}^{-1} - \psi \rangle_{\mathcal{I}_h^2} \\
&+ \langle (\boldsymbol{q}_h^1 \circ \boldsymbol{\phi}^{-1}) \cdot \boldsymbol{n}^2 - \boldsymbol{E}_{\boldsymbol{q}_h^1} \cdot \boldsymbol{n}^2, \psi \circ \boldsymbol{\phi}^{-1} \rangle_{\mathcal{I}_h^2} \\
=& \langle \widehat{u}_h^2, \boldsymbol{\varphi} \cdot \boldsymbol{n}^2 - (\boldsymbol{\varphi} \circ \boldsymbol{\phi}^{-1}) \cdot \boldsymbol{n}^2 \rangle_{\mathcal{I}_h^2} - \langle \widetilde{u}_h^2 \circ \boldsymbol{\phi}^{-1} - \widehat{u}_h^2, (\boldsymbol{\varphi} \circ \boldsymbol{\phi}^{-1}) \cdot \boldsymbol{n}^2 \rangle_{\mathcal{I}_h^2} \\
&+ \langle (\boldsymbol{q}_h^1 \circ \boldsymbol{\phi}^{-1}) \cdot \boldsymbol{n}^2 - \boldsymbol{E}_{\boldsymbol{q}_h^1} \cdot \boldsymbol{n}^2, \psi \circ \boldsymbol{\phi}^{-1} \rangle_{\mathcal{I}_h^2} + \langle \widehat{\boldsymbol{q}}_h^2 \cdot \boldsymbol{n}^2, \psi \circ \boldsymbol{\phi}^{-1} - \psi \rangle_{\mathcal{I}_h^2}.
\end{aligned}$$

In addition, by (20),

$$\begin{aligned}
\langle \widehat{\boldsymbol{q}}_h^2 \cdot \boldsymbol{n}^2, \psi \circ \boldsymbol{\phi}^{-1} - \psi \rangle_{\mathcal{I}_h^2} =& \langle \boldsymbol{q}_h^2 \cdot \boldsymbol{n}^2, \psi \circ \boldsymbol{\phi}^{-1} - \psi \rangle_{\mathcal{I}_h^2} + \langle \tau (u_h^2 - \widehat{u}_h^2), \psi \circ \boldsymbol{\phi}^{-1} - \psi \rangle_{\mathcal{I}_h^2} \\
=& - \langle |\sigma|^{-1} (\widetilde{u}_h^2 \circ \boldsymbol{\phi}^{-1} - \widehat{u}_h^2), \psi \circ \boldsymbol{\phi}^{-1} - \psi \rangle_{\mathcal{I}_h^2} - \langle \Lambda_{\boldsymbol{q}_h^2}^2, \psi \circ \boldsymbol{\phi}^{-1} - \psi \rangle_{\mathcal{I}_h^2} \\
&+ \langle \tau (u_h^2 - \widehat{u}_h^2), \psi \circ \boldsymbol{\phi}^{-1} - \psi \rangle_{\mathcal{I}_h^2},
\end{aligned}$$

which implies that

$$\begin{aligned}
\mathbb{T}_u^1 + \mathbb{T}_u^2 =& \langle \widehat{u}_h^2, \boldsymbol{\varphi} \cdot \boldsymbol{n}^2 - (\boldsymbol{\varphi} \circ \boldsymbol{\phi}^{-1}) \cdot \boldsymbol{n}^2 \rangle_{\mathcal{I}_h^2} - \langle \widetilde{u}_h^2 \circ \boldsymbol{\phi}^{-1} - \widehat{u}_h^2, (\boldsymbol{\varphi} \circ \boldsymbol{\phi}^{-1}) \cdot \boldsymbol{n}^2 \rangle_{\mathcal{I}_h^2} \\
&+ \langle (\boldsymbol{q}_h^1 \circ \boldsymbol{\phi}^{-1}) \cdot \boldsymbol{n}^2 - \boldsymbol{E}_{\boldsymbol{q}_h^1} \cdot \boldsymbol{n}^2, \psi \circ \boldsymbol{\phi}^{-1} \rangle_{\mathcal{I}_h^2} \\
&- \langle |\sigma|^{-1} (\widetilde{u}_h^2 \circ \boldsymbol{\phi}^{-1} - \widehat{u}_h^2), \psi \circ \boldsymbol{\phi}^{-1} - \psi \rangle_{\mathcal{I}_h^2} - \langle \Lambda_{\boldsymbol{q}_h^2}^2, \psi \circ \boldsymbol{\phi}^{-1} - \psi \rangle_{\mathcal{I}_h^2} \\
&+ \langle \tau (u_h^2 - \widehat{u}_h^2), \psi \circ \boldsymbol{\phi}^{-1} - \psi \rangle_{\mathcal{I}_h^2} = \sum_{i=1}^{5} \mathbb{S}_i,
\end{aligned}$$

where

$$\mathbb{S}_1 := -\langle |\sigma|^{-1/2}(\widetilde{u}_h^2 \circ \boldsymbol{\phi}^{-1} - \widehat{u}_h^2), |\sigma|^{1/2}(\boldsymbol{\varphi} \circ \boldsymbol{\phi}^{-1}) \cdot \boldsymbol{n}^2 + |\sigma|^{-1/2}(-\psi \circ \boldsymbol{\phi}^{-1} + \psi)\rangle_{\mathcal{I}_h^2},$$
$$\mathbb{S}_2 := \langle \widehat{u}_h^2, \boldsymbol{\varphi} \cdot \boldsymbol{n}^2 - (\boldsymbol{\varphi} \circ \boldsymbol{\phi}^{-1}) \cdot \boldsymbol{n}^2 \rangle_{\mathcal{I}_h^2},$$
$$\mathbb{S}_3 := \langle (\boldsymbol{q}_h^1 \circ \boldsymbol{\phi}^{-1}) \cdot \boldsymbol{n}^2 - \boldsymbol{E}_{\boldsymbol{q}_h^1} \cdot \boldsymbol{n}^2, \psi \circ \boldsymbol{\phi}^{-1} \rangle_{\mathcal{I}_h^2},$$
$$\mathbb{S}_4 := -\langle \Lambda^2_{\boldsymbol{q}_h^2}, \psi \circ \boldsymbol{\phi}^{-1} - \psi \rangle_{\mathcal{I}_h^2},$$
$$\mathbb{S}_5 := \langle \tau(u_h^2 - \widehat{u}_h^2), \psi \circ \boldsymbol{\phi}^{-1} - \psi \rangle_{\mathcal{I}_h^2}$$

We now bound each of these terms by the Cauchy-Schwarz inequality, the estimates in Lemma 1 and the regularity assumption (27):

$$\begin{aligned}
\mathbb{S}_1 &\lesssim R_2\, h_2 \||\sigma|^{-1/2}(\widetilde{u}_h^2 \circ \boldsymbol{\phi}^{-1} - \widehat{u}_h^2)\|_{\mathcal{I}_h^2} \|\psi\|_{H^2(\Omega)} && \lesssim R_2\, h_2 \||\sigma|^{-1/2}(\widetilde{u}_h^2 \circ \boldsymbol{\phi}^{-1} - \widehat{u}_h^2)\|_{\mathcal{I}_h^2} \|\Theta\|_{\Omega},\\
\mathbb{S}_2 &\lesssim \||\sigma|^{1/2}\widehat{u}_h^2\|_{\mathcal{I}_h^2} \|\boldsymbol{\varphi}\|_{\boldsymbol{H}^1(\Omega)} && \lesssim \||\sigma|^{1/2}\widehat{u}_h^2\|_{\mathcal{I}_h^2} \|\Theta\|_{\Omega},\\
\mathbb{S}_3 &\lesssim \max_{e \in \mathcal{I}_h^2}(r_e h_{K_e}^{-1/2} C_e^{ext})\, \|\boldsymbol{q}_h^1\|_{\mathcal{I}_h^2} \|\psi \circ \boldsymbol{\phi}^{-1}\|_{\mathcal{I}_h^2} && \lesssim \max_{e \in \mathcal{I}_h^2}(r_e h_{K_e}^{-1/2} C_e^{ext})\, \|\boldsymbol{q}_h^1\|_{\mathcal{I}_h^2} \|\Theta\|_{\Omega},\\
\mathbb{S}_4 &\lesssim (R_2 h_2)^{1/2} \||\sigma|^{1/2} \Lambda^2_{\boldsymbol{q}_h^2}\|_{\mathcal{I}_h^2} \|\psi\|_{H^1(\Omega)} && \lesssim (R_2 h_2)^{1/2} \||\sigma|^{1/2} \Lambda^2_{\boldsymbol{q}_h^2}\|_{\mathcal{I}_h^2} \|\Theta\|_{\Omega},\\
\mathbb{S}_5 &\lesssim R_2\, h_2\, \tau^{1/2} \|\tau(u_h^2 - \widehat{u}_h^2)\|_{\mathcal{I}_h^2} \|\psi\|_{H^1(\Omega)} && \lesssim R_2\, h_2\, \tau^{1/2} \|\tau(u_h^2 - \widehat{u}_h^2)\|_{\mathcal{I}_h^2} \|\Theta\|_{\Omega}.
\end{aligned}$$

In addition, by (24) and noticing that $|\sigma(\boldsymbol{x}^2)| \leq r_e h_{K_e}$ for all $\boldsymbol{x}^2 \in e$ and $e \in \mathcal{I}_h^2$, S_2 can be bounded as

$$\mathbb{S}_2 \lesssim \left(R_2^{1/2} h_2 \|\boldsymbol{q}_h^2\|_{\Omega_h^2} + R_2^{1/2} \|u_h^2\|_{\Omega_h^2} + R_2^{1/2} h_2 \|\boldsymbol{g}^2\|_{\Omega_h^2} \right) \|\Theta\|_{\Omega}.$$

Also, by the estimate in (10a), we have $\mathbb{S}_4 \lesssim R_2^2 h_2^{1/2} \max_{e \in \mathcal{I}_h^2}(C_e^{ext} C_e^{inv}) \|\boldsymbol{q}_h^2\|_{\Omega_h^2} \|\Theta\|_{\Omega}$.

In summary, combining (29) with the bound for $\mathbb{S}_i\, (i = 1, ..., 5)$ and noticing that

$$\|\boldsymbol{\Pi}_{\boldsymbol{V}^i} \boldsymbol{\varphi} - \boldsymbol{\varphi}\|_{\Omega_h^i} \leq C_{reg} h_i \|\Theta\|_{\Omega},$$

by (4a), we obtain

$$\begin{aligned}
\sum_{i=1}^{2} (u_h^i, \Theta)_{\Omega_h^i} \lesssim & \|\Theta\|_{\Omega} \left(R_2 h_2 + R_2^{1/2} h_2 + \max_{e \in \mathcal{I}_h^2}(r_e h_{K_e}^{-1/2} C_e^{ext}) + R_2^2 h_2^{1/2} \max_{e \in \mathcal{I}_h^2} C_e^{ext} C_e^{inv} + R_2 h_2 \tau^{1/2} + h_1 + h_2 \right) \\
& \left(\||\sigma|^{-1/2}(\widetilde{u}_h^2 \circ \boldsymbol{\phi}^{-1} - \widehat{u}_h^2)\|_{\mathcal{I}_h^2} + \|\tau^{1/2}(u_h^2 - \widehat{u}_h^2)\|_{\mathcal{I}_h^2} + \sum_{i=1}^{2} \|\boldsymbol{q}_h^i\|_{\Omega_h^i} \right) \\
& + R_2^{1/2} \|u_h^2\|_{\Omega_h^2} \|\Theta\|_{\Omega} + R_2^{1/2} h_2 \|\boldsymbol{g}^2\|_{\Omega_h^2} \|\Theta\|_{\Omega}.
\end{aligned}$$

Then, we take $\Theta = \left\{ \begin{array}{lll} u_h^1 & \text{in} & \Omega_h^1 \\ u_h^2 & \text{in} & \Omega_h^2 \end{array} \right.$ and we conclude that there exists $C_2 > 0$, independent of the meshsize, such that

$$\begin{aligned}
\left(\sum_{i=1}^{2} \|u_h^i\|^2_{\Omega_h^i} \right)^{1/2} \leq & C_2 \left(R_2 h_2 + R_2^{1/2} h_2 + \max_{e \in \mathcal{I}_h^2}(r_e h_{K_e}^{-1/2} C_e^{ext}) + R_2^2 h_2^{1/2} \max_{e \in \mathcal{I}_h^2} C_e^{ext} C_e^{inv} + R_2 h_2 \tau^{1/2} + h_1 + h_2 \right) \\
& \left(\||\sigma|^{-1/2}(\widetilde{u}_h^2 \circ \boldsymbol{\phi}^{-1} - \widehat{u}_h^2)\|_{\mathcal{I}_h^2} + \|\tau^{1/2}(u_h^2 - \widehat{u}_h^2)\|_{\mathcal{I}_h^2} + \sum_{i=1}^{2} \|\boldsymbol{q}_h^i\|_{\Omega_h^i} \right) \\
& + C_2 R_2^{1/2} \|u_h^2\|_{\Omega_h^2} + C_2 R_2^{1/2} h_2 \|\boldsymbol{g}^2\|_{\Omega_h^2}.
\end{aligned}$$

The result follows by considering Assumptions (A.4), (A.6) and (A.7). □

3.3 Proof of Theorem 2

Proof. Combining the estimates in Lemmas 3 and 4 we obtain (17b). In addition, by Lemma 3 and the estimate in Lemma 4 we have

$$\begin{aligned}\sum_{i=1}^{2}\|\boldsymbol{q}_h^i\|_{\Omega_h^i}^2+&\|\tau^{1/2}(u_h^i-\widehat{u}_h^i)\|_{\partial\Omega_h^i}^2+\||\sigma|^{-1/2}\left(\widetilde{u}_h^2\circ\boldsymbol{\phi}^{-1}-\widehat{u}_h^2\right)\|_{\mathcal{I}_h^2}^2\\ &\lesssim(1+\beta^2h_2^{2\alpha-2})\left(\beta\left(h_2^{2\alpha-1}+h_2^{\alpha+1}+h_2^{2(\alpha+1)}\tau\right)+h_1^2+h_2^2\right)\left(\|f\|_\Omega^2+\sum_{i=1}^{2}\|\boldsymbol{g}^i\|_{\Omega_h^i}^2\right)\\ &\quad+\|f\|_\Omega^2+(2+\beta h_2)\sum_{i=1}^{2}\|\boldsymbol{g}^i\|_{\Omega_h^i}^2+(\beta^3h_2^{3\alpha}+\beta h_2^{2+\alpha})\|\boldsymbol{g}^2\|_{\Omega_h^2}^2,\end{aligned}$$

which, after recalling that $h_1, h_2 < 1$ and $\alpha > 1/2$, implies (17a).

□

4 Error estimates

Let us proceed now to derive the error estimates of the proposed method (12). To that end, we employ the stability estimate deduced in previous sections.

Let us consider the solution $(\boldsymbol{q}, u)$ (1). For $i \in \{1, 2\}$ we introduce the projection of the errors $\boldsymbol{\varepsilon}^{\boldsymbol{q}^i} := \boldsymbol{\Pi}_{\boldsymbol{V}^i}\boldsymbol{q} - \boldsymbol{q}_h^i$, $\varepsilon^{u^i} := \Pi_{W^i}u - u_h^i$ and $\varepsilon^{\widehat{u}^i} := P_{M^i}u - \widehat{u}_h^i$, where we P_{M^i} is the L^2 projection into M_h^i; and the error of the projections $\boldsymbol{I}^{\boldsymbol{q}^i} := \boldsymbol{q} - \boldsymbol{\Pi}_{\boldsymbol{V}^i}\boldsymbol{q}$ and $I^{u^i} := u - \Pi_{W^i}u$. Using these quantities we can decompose the HDG error $\boldsymbol{q} - \boldsymbol{q}_h^i = \boldsymbol{\varepsilon}^{\boldsymbol{q}^i} + \boldsymbol{I}^{\boldsymbol{q}^i}$ and $u - u_h^i = \varepsilon^{u^i} + I^{u^i}$; and then the projection of the errors satisfies

$$(\boldsymbol{\varepsilon}^{\boldsymbol{q}^i}, \boldsymbol{v})_{\Omega_h^i} - (\varepsilon^{u^i}, \nabla\cdot\boldsymbol{v})_{\Omega_h^i} + \langle\widehat{u}_h^i, \boldsymbol{v}\cdot\boldsymbol{n}^i\rangle_{\partial\Omega_h^i} = -(\boldsymbol{I}^{\boldsymbol{q}^i}, \boldsymbol{v})_{\Omega_h^i}, \tag{30a}$$

$$-(\boldsymbol{\varepsilon}^{\boldsymbol{q}^i}, \nabla w)_{\Omega_h^i} + \langle\widehat{\boldsymbol{\varepsilon}^{\boldsymbol{q}^i}}\cdot\boldsymbol{n}^i, w\rangle_{\partial\Omega_h^i} = 0 \tag{30b}$$

$$\langle\widehat{\boldsymbol{\varepsilon}^{\boldsymbol{q}^i}}\cdot\boldsymbol{n}^i, \mu\rangle_{\partial\Omega_h^i\setminus\Gamma_h^i} = 0, \tag{30c}$$

$$\langle\varepsilon^{\widehat{u}^i}, \mu\rangle_{\Gamma_h^i\setminus\mathcal{I}_h^i} = 0, \tag{30d}$$

for all $(\boldsymbol{v}, w, \mu) \in \boldsymbol{V}_h^i \times W_h^i \times M_h^i$, where $\widehat{\boldsymbol{\varepsilon}^{\boldsymbol{q}^i}}\cdot\boldsymbol{n}^i := \boldsymbol{\varepsilon}^{\boldsymbol{q}^i}\cdot\boldsymbol{n}^i + \tau(\varepsilon^{u^i} - \varepsilon^{\widehat{u}^i})$ on $\partial\Omega_h^i$; and

$$\langle\varepsilon^{\widehat{u}^1} - \varepsilon^{\widetilde{u}^2}, \mu\rangle_{\mathcal{I}_h^1} = 0, \qquad \forall\mu \in M_h^1 \tag{30e}$$

$$\langle\widehat{\boldsymbol{\varepsilon}^{\boldsymbol{q}^2}}\cdot\boldsymbol{n}^2 + \varepsilon^{\widetilde{q}^2}, \mu\rangle_{\mathcal{I}_h^2} = 0, \qquad \forall\mu \in M_h^2 \tag{30f}$$

where $\varepsilon^{\widetilde{u}^2} := P_{M^1}u - \widetilde{u}_h^2$ and $\varepsilon^{\widetilde{q}^2} := \boldsymbol{q}^2\cdot\boldsymbol{n}^2 - \widetilde{q}_h^1$.

By the stability estimate (17a) applied to (30), where $\boldsymbol{I}^{\boldsymbol{q}^i}$ and 0 play the role of $\boldsymbol{g}^i$ and f respectively, we obtain

$$\sum_{i=1}^{2}\|\boldsymbol{\varepsilon}^{\boldsymbol{q}^i}\|_{\Omega_h^i}^2 + \|\tau^{1/2}(\varepsilon^{u^i} - \varepsilon^{\widehat{u}^i})\|_{\partial\Omega_h^i}^2 + \||\sigma|^{-1/2}\big(\varepsilon^{\widetilde{u}^2}\circ\boldsymbol{\phi}^{-1} - \varepsilon^{\widehat{u}^2}\big)\|_{\mathcal{I}_h^2}^2 \lesssim (\beta\,(1+\tau)+1)\sum_{i=1}^{2}\|\boldsymbol{I}^{\boldsymbol{q}^i}\|_{\Omega_h^i}^2. \tag{31}$$

Moreover, by (17b),

$$\sum_{i=1}^{2}\|\varepsilon^{u^i}\|_{\Omega_h^i}^2 \lesssim \left(\beta\left(h_2^{2\alpha-1}+h_2^{\alpha+1}+h_2^{2(\alpha+1)}\tau\right)+h_1^2+h_2^2\right)\left(\sum_{i=1}^{2}\|\boldsymbol{I}^{\boldsymbol{q}^i}\|_{\Omega_h^i}^2\right). \tag{32}$$

Finally, by (31) and (32) and the properties of the HDG projectors (c.f. (4)), we obtain the following result.

Theorem 5. *Suppose Assumptions (A) hold true, $\alpha > 1/2$ and elliptic regularity holds. If τ is of order one and $(\boldsymbol{q}, u) \in \boldsymbol{H}^{l_{\boldsymbol{q}}+1}(\Omega) \times H^{l_u+1}(\Omega)$, then*

$$\left(\sum_{i=1}^{2} \|\boldsymbol{q} - \boldsymbol{q}_h^i\|_{\Omega_h^i}^2\right)^{1/2} + \left(\sum_{i=1}^{2} \|u - u_h^i\|_{\Omega_h^i}^2\right)^{1/2} \lesssim \left(\sum_{i=1}^{2} h_i^{2(l_{\boldsymbol{q}}+1)} \|\boldsymbol{q}\|_{\Omega_h^i}^2\right)^{1/2} + \left(\sum_{i=1}^{2} h_i^{2(l_u+1)} \|u\|_{\Omega_h^i}^2\right)^{1/2}.$$

for all $h \in (0, 1)$.

Corollary 5.1. *Suppose the same assumptions of Theorem 5 hold. If $(\boldsymbol{q}, u) \in \boldsymbol{H}^{k+1}(\Omega) \times H^k(\Omega)$, then*

$$\left(\sum_{i=1}^{2} \|\boldsymbol{q} - \boldsymbol{q}_h^i\|_{\Omega_h^i}^2\right)^{1/2} + \left(\sum_{i=1}^{2} \|u - u_h^i\|_{\Omega_h^i}^2\right)^{1/2} \lesssim h_1^{k+1} + h_2^{k+1}.$$

We finish this section by showing the error estimates of a postprocessing of u_h^i $(i = 1, 2)$. In particular, as introduced by Stenberg [14], it is possible to define a locally post-processed function $(u_h^*)^i$ to be the piecewise polynomial function satisfying, for all $K \in \Omega_h^i$,

$$\begin{aligned} (u_h^*)^i &\in \mathbb{P}_{k+1}(K) \\ (\nabla(u_h^*)^i, \nabla w_h)_K &= (\boldsymbol{q}_h^i, \nabla w_h)_K \quad \forall\, w_h \in \mathbb{P}_{k+1}(K), \qquad (33a) \\ ((u_h^*)^i, 1)_K &= (u_h^i, 1)_K. \qquad (33b) \end{aligned}$$

In addition, under the assumptions of Corollary (5.1), the post-processed solution satisfies (cf. [4])

$$\|u - (u_h^*)^i\|_{\Omega_h^i} \lesssim \|\varepsilon^{u^i}\|_{\Omega_h^i} + h_i \|\boldsymbol{q}^i - \boldsymbol{q}_h^i\|_{\Omega_h^i} + h_i^{k+2} |\boldsymbol{q}|_{\boldsymbol{H}^{k+1}(\Omega_h^i)}.$$

Then, by (32), (4a) and Corollary (5.1),

$$\sum_{i=1}^{2} \|u - (u_h^*)^i\|_{\Omega_h^i}^2 \lesssim \left(\beta \left(h_2^{2\alpha-1} + h_2^{\alpha+1} + h_2^{2(\alpha+1)}\right) + h_1^2 + h_2^2\right)(h_1^{2(k+1)} + h_2^{2(k+1)}) + h_1^{2(k+2)} + h_2^{2(k+2)}.$$

Remark 6. *The above estimates indicates that, if $\beta = 0$ (i.e. no gap), the post-processed solution super-converges with order h_2^{k+2}, since $h_1 < h_2$. On the other hand, if $\beta \neq 0$ and then the order of convergence is $h_2^{k+1+\frac{1}{2}\min\{2\alpha-1, \alpha+1\}}$.*

5 Numerical Results

We consider four numerical examples to illustrate the convergence rates of the method. For all the examples we consider the physical domain Ω to be a square $[0, 1] \times [0, 1]$, which is approached by the computational domains $\Omega_h^1 \cup \Omega_h^2$. The four examples differ in the way the subdomains Ω_h^i are geometrically interfaced. We use the same manufactured solution $u(x, y) = \sin(\pi x) \sin\left[\pi(-0.2y^2 + 1.2y)\right]$, for all the numerical tests. The forcing term f, and the homogeneous Dirichlet boundary conditions applied on $x = \pm 1$ and $y = \pm 1$ are derived from this exact solution. The stabilization parameter τ is always set equal to one. Following [6, 7], we compute the errors

$$e_{\boldsymbol{q}} := \frac{1}{|\Omega_h|^{1/2}} \left(\sum_{i=1}^{2} \|\boldsymbol{q}^i - \boldsymbol{q}_h^i\|_{\Omega_h^i}^2\right)^{1/2}, \quad e_u := \frac{1}{|\Omega_h|^{1/2}} \left(\sum_{i=1}^{2} \|u^i - u_h^i\|_{\Omega_h^i}^2\right)^{1/2}$$

$$e_{u^*} := \frac{1}{|\Omega_h|^{1/2}} \left(\sum_{i=1}^{2} \|u^i - (u_h^*)^i\|_{\Omega_h^i}^2\right)^{1/2},$$

where $|\Omega_h| = |\Omega_h^1| + |\Omega_h^2|$ is the total volume of the computational domain. In addition, for each variable, we compute the experimental order of convergence defined as e.o.c. $= \log\left(e_{h_1}/e_{h_2}\right)/(h_1/h_2)$, where e_{h_1} and e_{h_2} are the errors associated to the corresponding variable considering two consecutive meshes with h_1 and h_2 elements, respectively.

5.1 Test cases with ratios $r_e = \mathcal{O}(h)$

For the first test, Ω_h^1 and Ω_h^2 are two symmetric uniform quadrilateral meshes separated by a flat interface centered at $y = 0.5$ and with a gap of thickness $h^2/2$. The computational domains are similar to the ones illustrated in Figure 5, although the gap used in the current example is smaller than the one depicted in Figure 5. Note that the area of the computational domain increases as the mesh is refined, which motivates the use of error norms rescaled with $|\Omega_h|^{1/2}$.

The ratio $r_e = h/2$ is uniform on the interface. According to the notation in Assumptions A, $\alpha = 1$ and $\beta = 2$, and all those assumptions are satisfied for h_2 small enough. Table 1 shows the errors and convergence rates for the approximate solution u_h, the approximate gradient $\boldsymbol{q}_h$, and the post-processed solution u_h^*. We observe that the HDG approximation of u and $\boldsymbol{q}$ converges with order $k+1$ as predicted by Corollary 5.1. We also observe an experimental order of convergence of $k+2$ for the post-processed solution, which is half a power better than the one stated in Remark 5.1.

k	mesh size h	e_u	e.o.c	$e_{\boldsymbol{q}}$	e.o.c	e_{u^*}	e.o.c
1	5.000e-01	1.20e-01	–	3.57e-01	–	5.89e-02	–
	2.500e-01	4.55e-02	1.40	1.43e-01	1.33	9.93e-03	2.57
	1.250e-01	1.40e-02	1.70	4.44e-02	1.68	1.49e-03	2.73
	6.250e-02	3.91e-03	1.84	1.24e-02	1.84	2.07e-04	2.85
	3.125e-02	1.03e-03	1.92	3.28e-03	1.92	2.72e-05	2.92
	1.562e-02	2.66e-04	1.96	8.43e-04	1.96	3.50e-06	2.96
	7.812e-03	6.74e-05	1.98	2.14e-04	1.98	4.43e-07	2.98
2	5.000e-01	3.32e-02	–	1.61e-01	–	2.48e-02	–
	2.500e-01	4.01e-03	3.05	1.44e-02	3.49	1.43e-03	4.11
	1.250e-01	5.58e-04	2.85	1.80e-03	3.00	7.46e-05	4.26
	6.250e-02	7.48e-05	2.90	2.37e-04	2.92	4.13e-06	4.18
	3.125e-02	9.69e-06	2.95	3.07e-05	2.95	2.41e-07	4.10
	1.562e-02	1.23e-06	2.97	3.90e-06	2.98	1.46e-08	4.05
	7.812e-03	1.55e-07	2.99	4.92e-07	2.99	8.94e-10	4.03
3	5.000e-01	2.32e-03	–	1.12e-02	–	1.77e-03	–
	2.500e-01	2.12e-04	3.46	8.73e-04	3.69	1.29e-04	3.78
	1.250e-01	1.35e-05	3.97	4.63e-05	4.24	4.11e-06	4.98
	6.250e-02	8.76e-07	3.95	2.82e-06	4.03	1.21e-07	5.08
	3.125e-02	5.61e-08	3.97	1.78e-07	3.98	3.63e-09	5.06
	1.562e-02	3.55e-09	3.98	1.13e-08	3.99	1.11e-10	5.04
	7.812e-03	2.23e-10	3.99	7.08e-10	3.99	3.13e-12	5.14

Table 1: History of convergence of the HDG method for a square domain with a flat interface, and $r_e = h/2$ ($\alpha = 1$ and $\beta = 2$).

For the second test, we now consider that Ω_h^1 and Ω_h^2 are connected via non-matching curved interfaces. The computational domains make use of isoparametric curved elements to represent two different curved interfaces. More specifically,

$$\begin{aligned} &\mathcal{I}_h^1 \ \text{ interpolates the curve } \ y(x) = 0.5 + 0.025\sin(4\pi x), \\ &\mathcal{I}_h^2 \ \text{ interpolates the curve } \ y(x) = 0.5 + \big(0.025 + h^2/2\big)\sin(4\pi x). \end{aligned}$$

The computational domains are similar to the ones illustrated in Figure 6, although the gap used in the current example is smaller than the one depicted in Figure 6. From the definitions of the computational interfaces, it is obvious that the two subdomains partially overlap and partially separate, with the width of both gaps and overlaps being bound by $h^2/2$. Therefore, $r_e \leq h/2$, and Assumption (A.4) holds with $\alpha = 1$ and $\beta = 2$. Assumption (A.3) is no longer exactly satisfied since the direction of the connecting segments

$\boldsymbol{m}$ deviates from the element normals. However, here $1-\boldsymbol{m}\cdot\boldsymbol{n}^1$ and $1-\boldsymbol{m}\cdot\boldsymbol{n}^2$ remain small all along the computational interfaces. Finally, all the other Assumptions A are satisfied for h_2 small enough. Note that no special treatment is applied in the overlapped regions, as the extrapolation operator (2) becomes a mere interpolation.

In Table 2 we show the results for this case and observe that the approximations of all the variables converge with order $k+1$, verifying Corollary 5.1, and the post-processed solution converges with order $k+2$. Interestingly, it seems that the use of curved elements, non-normal connecting segments, and overlapping regions does not downgrade the convergence rates observed for the previous case.

k	mesh size h	e_u	e.o.c	$e_{\boldsymbol{q}}$	e.o.c	e_{u^*}	e.o.c
1	5.000e-01	1.37e-01	–	3.68e-01	–	5.99e-02	–
	2.500e-01	4.68e-02	1.54	1.45e-01	1.35	1.11e-02	2.43
	1.250e-01	1.43e-02	1.71	4.57e-02	1.66	1.71e-03	2.70
	6.250e-02	3.96e-03	1.85	1.29e-02	1.83	2.39e-04	2.84
	3.125e-02	1.05e-03	1.92	3.49e-03	1.88	3.17e-05	2.91
	1.562e-02	2.70e-04	1.96	9.30e-04	1.91	4.13e-06	2.94
	7.812e-03	6.86e-05	1.98	2.46e-04	1.92	5.30e-07	2.96
2	5.000e-01	2.63e-02	–	8.43e-02	–	3.51e-03	–
	2.500e-01	5.22e-03	2.33	2.15e-02	1.97	6.01e-04	2.55
	1.250e-01	6.38e-04	3.03	2.50e-03	3.11	2.38e-05	4.66
	6.250e-02	8.48e-05	2.91	3.45e-04	2.86	1.42e-06	4.07
	3.125e-02	1.11e-05	2.93	4.69e-05	2.88	8.99e-08	3.98
	1.562e-02	1.42e-06	2.96	6.22e-06	2.91	5.75e-09	3.97
	7.812e-03	1.81e-07	2.98	8.08e-07	2.95	3.67e-10	3.97
3	5.000e-01	1.33e-02	–	1.51e-01	–	1.18e-02	–
	2.500e-01	4.50e-04	4.89	2.45e-03	5.95	6.51e-05	7.50
	1.250e-01	4.56e-05	3.30	2.62e-04	3.22	2.23e-06	4.87
	6.250e-02	3.17e-06	3.85	1.83e-05	3.84	6.16e-08	5.18
	3.125e-02	2.09e-07	3.92	1.23e-06	3.89	1.94e-09	4.99
	1.562e-02	1.35e-08	3.95	8.07e-08	3.93	6.13e-11	4.98
	7.812e-03	8.62e-10	3.97	5.19e-09	3.96	1.94e-12	4.98

Table 2: History of convergence of the HDG method for a square domain with partially overlapping curved meshes and with $r_e < h/2$ ($\alpha = 1$ and $\beta = 2$).

5.2 Test cases with $r_e = \mathcal{O}(1)$

We now consider two new numerical examples replicating the two first examples with wider mesh gaps.

The third example is similar to the first one, but with a gap width now equal to $h/4$ as shown in Figure 5. We present the numerical results in Table 3. Even though this scenario is not covered by our theory since now $r_e = 1/4$ and $\alpha = 0$, we observe that all the approximate variables still converge with the optimal order $k+1$. However, the superconvergence of the post-processed variable is lost.

Finally, we set a fourth example similar to the second one, by changing the definition of the computational interface

$$\mathcal{I}_h^2 \;\text{ interpolating the curve }\; y(x) = 0.5 + (0.025 + h/4)\sin(4\pi x),$$

such that now $r_e \leq 1/4$. Since $\alpha = 0$, this case is still not covered by the analysis. The computational domains are illustrated in Figure 6. In Table 4, we show the results for this case and observe that the approximations of all the variables converge with order $k+1$.

Although there is not yet an analysis for the case $r_e = \mathcal{O}(1)$, i.e $\alpha = 0$, it seems that our method provides optimal orders of convergence for both the approximated solution and the approximated gradient.

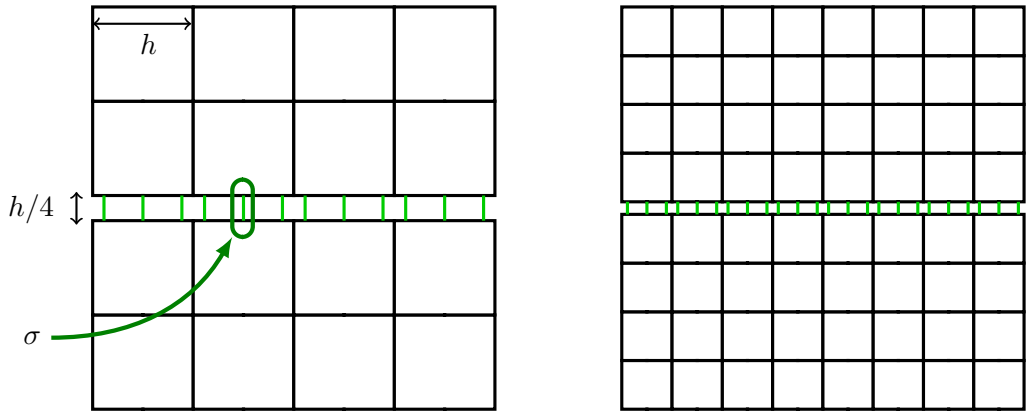

Figure 5: Two of the meshes used for the third numerical example, with $r_e = 1/4$ and flat interfaces. $h = 1/4$ for the left mesh, and $h = 1/8$ for the right one. Note the connecting segments σ at the interface Gauss points drawn in green (here, $k = 2$).

k	mesh size h	e_u	e.o.c	$e_{\boldsymbol{q}}$	e.o.c	e_{u^*}	e.o.c
1	5.000e-01	1.20e-01	–	3.57e-01	–	5.89e-02	–
	2.500e-01	4.43e-02	1.44	1.41e-01	1.34	8.95e-03	2.72
	1.250e-01	1.38e-02	1.69	4.42e-02	1.68	1.15e-03	2.96
	6.250e-02	3.88e-03	1.83	1.24e-02	1.83	2.63e-04	2.13
	3.125e-02	1.03e-03	1.91	3.30e-03	1.91	8.31e-05	1.66
	1.562e-02	2.66e-04	1.95	8.52e-04	1.96	2.40e-05	1.79
	7.812e-03	6.76e-05	1.98	2.16e-04	1.98	6.44e-06	1.90
2	5.000e-01	3.32e-02	–	1.61e-01	–	2.48e-02	–
	2.500e-01	4.96e-03	2.74	2.20e-02	2.87	3.46e-03	2.84
	1.250e-01	6.74e-04	2.88	2.79e-03	2.98	4.19e-04	3.05
	6.250e-02	8.83e-05	2.93	3.50e-04	2.99	5.02e-05	3.06
	3.125e-02	1.13e-05	2.96	4.39e-05	3.00	6.09e-06	3.04
	1.562e-02	1.43e-06	2.98	5.50e-06	3.00	7.49e-07	3.02
	7.812e-03	1.80e-07	2.99	6.88e-07	3.00	9.27e-08	3.01
3	5.000e-01	2.32e-03	–	1.12e-02	–	1.77e-03	–
	2.500e-01	4.03e-04	2.53	2.06e-03	2.45	3.72e-04	2.25
	1.250e-01	3.37e-05	3.58	1.71e-04	3.59	3.15e-05	3.56
	6.250e-02	2.35e-06	3.84	1.18e-05	3.85	2.20e-06	3.84
	3.125e-02	1.54e-07	3.93	7.72e-07	3.94	1.44e-07	3.93
	1.562e-02	9.84e-09	3.97	4.92e-08	3.97	9.19e-09	3.97
	7.812e-03	6.21e-10	3.99	3.10e-09	3.99	5.80e-10	3.99

Table 3: History of convergence of the HDG method for a square domain with a flat interface and $r_e = 1/4$ ($\alpha = 0$ and $\beta = 1/4$).

Acknowledgement

Sébastien Terrana, Ngoc-Cuong Nguyen and Jaime Peraire gratefully acknowledge the NASA for supporting this work under grant number NNX16AP15A. Manuel Solano was partially funded by CONICYT–Chile through FONDECYT projects 1160320, 1200569 and by Project AFB170001 of the PIA Program: Concurso Apoyo a Centros Científicos y Tecnológicos de Excelencia con Financiamiento Basal.

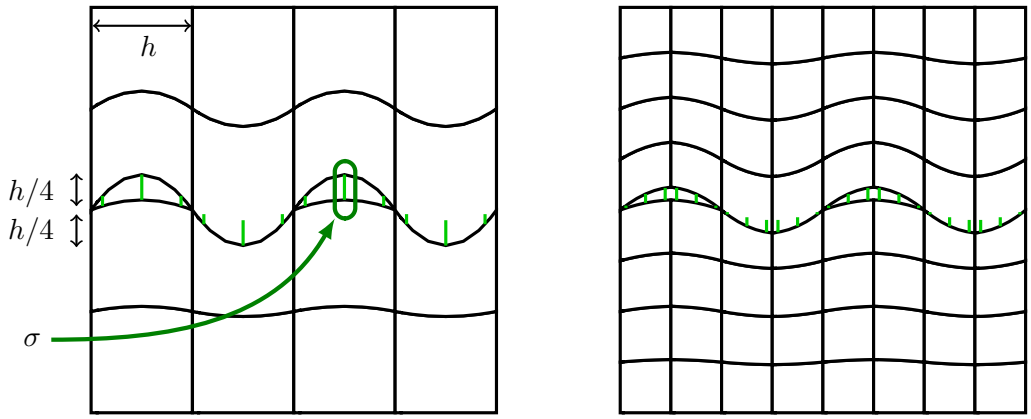

Figure 6: Two of the meshes used for the fourth numerical example, with curved elements, $k = 2$ being displayed here. $h = 1/4$ for the left mesh, and $h = 1/8$ for the right one. Note the length of the connecting segments is bounded by $h/4$, in both the overlap and the gap areas.

k	mesh size h	e_u	e.o.c	$e_{\boldsymbol{q}}$	e.o.c	e_{u^*}	e.o.c
1	5.000e-01	1.37e-01	–	3.68e-01	–	5.99e-02	–
	2.500e-01	4.68e-02	1.54	1.45e-01	1.35	1.11e-02	2.43
	1.250e-01	1.45e-02	1.69	4.70e-02	1.62	1.67e-03	2.74
	6.250e-02	4.00e-03	1.86	1.32e-02	1.84	2.21e-04	2.92
	3.125e-02	1.05e-03	1.92	3.55e-03	1.89	2.83e-05	2.96
	1.562e-02	2.71e-04	1.96	9.42e-04	1.91	4.83e-06	2.55
	7.812e-03	6.87e-05	1.98	2.48e-04	1.93	1.25e-06	1.95
2	5.000e-01	2.63e-02	–	8.43e-02	–	3.51e-03	–
	2.500e-01	6.69e-03	1.97	2.92e-02	1.53	1.07e-03	1.72
	1.250e-01	7.62e-04	3.13	3.29e-03	3.15	6.78e-05	3.98
	6.250e-02	9.34e-05	3.03	4.08e-04	3.01	7.93e-06	3.10
	3.125e-02	1.17e-05	3.00	5.17e-05	2.98	1.02e-06	2.96
	1.562e-02	1.47e-06	2.99	6.59e-06	2.97	1.31e-07	2.96
	7.812e-03	1.84e-07	3.00	8.37e-07	2.98	1.67e-08	2.97
3	5.000e-01	1.33e-02	–	1.51e-01	–	1.18e-02	–
	2.500e-01	8.88e-04	3.90	5.02e-03	4.92	1.74e-04	6.08
	1.250e-01	7.26e-05	3.61	4.00e-04	3.65	8.64e-06	4.33
	6.250e-02	4.39e-06	4.05	2.49e-05	4.01	5.28e-07	4.03
	3.125e-02	2.51e-07	4.13	1.46e-06	4.09	3.57e-08	3.89
	1.562e-02	1.50e-08	4.07	8.90e-08	4.04	2.36e-09	3.92
	7.812e-03	9.14e-10	4.03	5.51e-09	4.02	1.52e-10	3.95

Table 4: History of convergence of the HDG method for a square domain with partially overlapping curved meshes, and $r_e \leq 1/4$ ($\alpha = 0$ and $\beta = 1/4$).

Appendix

Proof of Lemma 1.

Proof. By a density argument, it is enough to show the first three estimates assuming $\psi \in C^\infty \cap H^2(\Omega)$. First, let $e \in \mathcal{I}_h^2$ and $\boldsymbol{x}^2$. By Taylor's theorem, we write

$$\psi(\boldsymbol{x}^2) = \psi(\boldsymbol{\phi}^{-1}(\boldsymbol{x}^2)) + |\sigma(\boldsymbol{x}^2)|\partial_{\boldsymbol{n}^2}\psi(\boldsymbol{\phi}^{-1}(\boldsymbol{x}^2)) + R_\psi(\boldsymbol{x}^2), \tag{34}$$

where the residual is given by $R_\psi(\boldsymbol{x}^2) := \displaystyle\int_0^{|\sigma(\boldsymbol{x}^2)|} (\sigma(\boldsymbol{x}^2) - s)\partial^2_{\boldsymbol{n}^2}\psi(\boldsymbol{x}^1 + s\boldsymbol{n}^2)\, ds$. By the Cauchy-Schwarz inequality, is it possible to obtain that $|R_\psi(\boldsymbol{x}^2)|^2 \leq \dfrac{|\sigma(\boldsymbol{x}^2)|^3}{3}\|\partial^2_{\boldsymbol{n}^2}\psi\|^2_{L^2(0,|\sigma(\boldsymbol{x}^2)|)}$. Then, since $\boldsymbol{\varphi} = -\nabla\psi$, from (34), we deduce

$$\Big(|\sigma(\boldsymbol{x}^2)|^{-1/2}(\psi(\boldsymbol{x}^2) - \psi(\boldsymbol{\phi}^{-1}(\boldsymbol{x}^2)) + |\sigma(\boldsymbol{x}^2)|^{1/2}\boldsymbol{\varphi}(\boldsymbol{\phi}^{-1}(\boldsymbol{x}^2))\cdot\boldsymbol{n}^2)\Big)^2 \leq \frac{|\sigma(\boldsymbol{x}^2)|^2}{3}\|\partial^2_{\boldsymbol{n}^2}\psi\|^2_{L^2(0,|\sigma(\boldsymbol{x}^2)|)}.$$

Integrating this expression along e and bounding the norm of the second derivatives by the H^2-norm, we obtain

$$\||\sigma|^{-1/2}(\psi - \psi\circ\boldsymbol{\phi}^{-1}) + |\sigma(\boldsymbol{x}^2)|^{1/2}(\boldsymbol{\varphi}\circ\boldsymbol{\phi}^{-1})\cdot\boldsymbol{n}^2)\|^2_e \leq \frac{1}{3}\max_{\boldsymbol{x}^2\in e}|\sigma(\boldsymbol{x}^2)|^2\ \|\psi\|^2_{H^2(\Omega)}.$$

Thus, since $|\sigma(\boldsymbol{x}^2)| \leq R_2h_2$, for all $\boldsymbol{x}^2 \in e$, (11a) follows. Similarly, from (34), we can bound

$$\begin{aligned}||\sigma(\boldsymbol{x}^2)|^{-1/2}(\psi(\boldsymbol{x}^2) - \psi(\boldsymbol{\phi}^{-1}(\boldsymbol{x}^2)))|^2 &\leq 2|\sigma(\boldsymbol{x}^2)|\ |\partial_{\boldsymbol{n}^2}\psi(\boldsymbol{\phi}^{-1}(\boldsymbol{x}^2))|^2 + 2|\sigma(\boldsymbol{x}^2)|^{-1}|R_\psi(\boldsymbol{x}^2)|^2\\ &\leq 2|\sigma(\boldsymbol{x}^2)|\ |\partial_{\boldsymbol{n}^2}\psi(\boldsymbol{\phi}^{-1}(\boldsymbol{x}^2))|^2 + \frac{2}{3}|\sigma(\boldsymbol{x}^2)|^2\|\partial^2_{\boldsymbol{n}^2}\psi\|^2_{L^2(0,|\sigma(\boldsymbol{x}^2)|)},\end{aligned}$$

where, for the last step, we have used the fact that $\boldsymbol{\varphi} = -\nabla\psi$. Thus, integrating previous expression over e, considering that $|\sigma(\boldsymbol{x}^2)|^2 \leq |\sigma(\boldsymbol{x}^2)|$ and bounding the norm of the second derivatives by the H^2-norm, we conclude

$$\||\sigma(\boldsymbol{x}^2)|^{-1/2}(\psi(\boldsymbol{x}^2) - \psi(\boldsymbol{\phi}^{-1}(\boldsymbol{x}^2)))\|^2_e \lesssim \max_{\boldsymbol{x}^2\in e}|\sigma(\boldsymbol{x}^2)|\ \|\psi\|^2_{H^2(\Omega)},$$

which implies (11a), since $\max\limits_{\boldsymbol{x}^2\in e} \leq R_2h_2$.

Now, to show (11c), again by Taylor's theorem, we write

$$\boldsymbol{\varphi}(\boldsymbol{x}^2)\cdot\boldsymbol{n}^2 = \boldsymbol{\varphi}(\boldsymbol{\phi}^{-1}(\boldsymbol{x}^2))\cdot\boldsymbol{n}^2 + R_{\boldsymbol{\varphi}}(\boldsymbol{x}^2),$$

where $R_{\boldsymbol{\varphi}}(\boldsymbol{x}^2) := \displaystyle\int_0^{|\sigma(\boldsymbol{x}^2)|} \partial_{\boldsymbol{n}^2}(\boldsymbol{\varphi}(\boldsymbol{x}^1 + s\boldsymbol{n}^2)\cdot\boldsymbol{n}^2)\, ds$. The estimate in (11c) follows by the same arguments employed before and noticing that $|R_{\boldsymbol{\varphi}}(\boldsymbol{x}^2)|^2 \leq |\sigma(\boldsymbol{x}^2)|\|\partial_{\boldsymbol{n}^2}(\boldsymbol{\varphi}\cdot\boldsymbol{n}^2)\|^2_{L^2(0,|\sigma(\boldsymbol{x}^2)|)}$.

Finally, let $e \in \mathcal{I}_h^2$ with K_e the element where e belongs. If $p \in \mathbb{P}(K_e)$, repeating the same arguments as above, for $\boldsymbol{x}^2 \in e$ is possible to deduce that

$$|p(\boldsymbol{x}^2) - p(\boldsymbol{\phi}(\boldsymbol{x}^2))|^2 \leq |\sigma(\boldsymbol{x}^2)|\ \|\nabla p\|^2_{L^2(0,|\sigma(\boldsymbol{x}^2)|)}.$$

Integrating along e and recalling the definition of K_e^{ext} in (5), we have

$$\|p - p\circ\boldsymbol{\phi}^{-1}\|^2_e \leq |\sigma(\boldsymbol{x}^2)|\ \|\nabla p\|^2_{K_e^{ext}} \leq |\sigma(\boldsymbol{x}^2)|\ (C_e^{ext})^2\ r_e\ h_{K_e}^{-2}\ \|p\|^2_{K_e},$$

where we used the definition of C_e^{ext} (cf. (8)) and the inverse inequality on K_e. Thus, (11d) follows after noticing that $|\sigma(\boldsymbol{x}^2)| \leq r_e h_{K^e}$. □

References

[1] G. Bfer, *An isoparametric joint/interface element for finite element analysis*, International Journal for Numerical Methods in Engineering, 21 (1985), pp. 585–600.

[2] J. Cheung, M. Gunzburger, P. Bochev, and M. Perego, *An optimally convergent higher-order finite element coupling method for interface and domain decomposition problems*, Results in Applied Mathematics, 6 (2020), p. 100094.

[3] J. Cheung, M. Perego, P. Bochev, and M. Gunzburger, *Optimally accurate higher-order finite element methods for polytopial approximations of domains with smooth boundaries.*, Mathematics of Computation, 88 (2019), p. 2187219.

[4] B. Cockburn, J. Gopalakrishnan, and F.-J. Sayas, *A projection-based error analysis of HDG methods*, Mathematics of Computation, 79 (2010), pp. 1351–1367.

[5] B. Cockburn, W. Qiu, and K. Shi, *Conditions for superconvergence of hdg methods for second-order elliptic problems*, Mathematics of Computation, 81 (2012), pp. 1327–1353.

[6] B. Cockburn, W. Qiu, and M. Solano, *A priori error analysis for HDG methods using extensions from subdomains to achieve boundary conformity*, Mathematics of Computation, 83 (2014), pp. 665–699.

[7] B. Cockburn and M. Solano, *Solving Dirichlet boundary-value problems on curved domains by extensions from subdomains*, SIAM Journal on Scientific Computing, 34 (2012), pp. A497–A519.

[8] B. Cockburn and M. Solano, *Solving convection-diffusion problems on curved domains by extensions from subdomains*, Journal of Scientific Computing, 59 (2014), pp. 512–543.

[9] M. Dittmann, S. Schu, B. Wohlmuth, and C. Hesch, *Weak cn coupling for multipatch isogeometric analysis in solid mechanics*, International Journal for Numerical Methods in Engineering, 118 (2019), pp. 678–699.

[10] B. Flemisch, J. Melenk, and B. Wohlmuth, *Mortar methods with curved interfaces*, Applied Numerical Mathematics, 54 (2005), pp. 339 – 361. Selected papers from the 16th Chemnitz Finite Element Symposium 2003.

[11] L. T. Huynh, N. Nguyen, J. Peraire, and B. Khoo, *A high-order hybridizable discontinuous galerkin method for elliptic interface problems*, International Journal for Numerical Methods in Engineering, 93 (2013), pp. 183–200.

[12] M. Lenoir, *Optimal isoparametric finite elements and error estimates for domains involving curved boundaries*, SIAM J. Numer. Anal., 23 (1986), pp. 562–580.

[13] W. Qiu, M. Solano, and P. Vega, *A high order HDG method for curved-interface problems via approximations from straight triangulations*, Journal of Scientific Computing, 69 (2016), pp. 1384–1407.

[14] R. Stenberg, *Postprocessing schemes for some mixed finite elements*, ESAIM: M2AN, 25 (1991), pp. 151–167.